Human-Structure Interaction in the TCF Bank Stadium and a Study of Parameter Estimation Algorithms

by

Manuel Aldaco Lopez

A Thesis Presented in Partial Fulfillment
of the Requirements for the Degree
Master of Science

Approved April 2014 by the
Graduate Supervisory Committee:

Keith Hjelmstad, Chair
Subramaniam Rajan
Apostolos Fafitis

ARIZONA STATE UNIVERSITY

May 2014

ABSTRACT

As more and more stadia structures nowadays are being built by making use of new high strength building materials which tend to be lighter than the “old” ones, composite systems and also the fact that engineers, contractors and clients want their structures as optimized as possible, in terms of minimal materials used, there is an inevitable side effect that comes with this. The result is that structures are more flexible, and thus they become susceptible to undergone vibration problems due to the action of dynamic loading. Pop/rock concerts, exhibitions, boxing matches, and so forth are staged to supplement the football/sport seasons. Consequently, stadia structures must resist not only static loading, but also dynamic loading, such as the human induced loads from various activities of the spectators which include, standing, jumping, stamping, clapping and dancing, particularly in response to touchdowns (in football matches) or musical beats (during concerts).

Active and passive models of humans are studied to see how they influence the response in TCF Bank Stadium for different ranges in excitation frequencies, by performing dynamic analyses and comparing the results with the ones obtained from static analysis.

Parameter estimation and system identification in mechanical sciences and structural engineering have become increasingly important areas of research in the last three decades. Many nondestructive testing methods are based on the concepts of system identification and parameter estimation.

In this document, two parameter estimation algorithms are studied, namely the Equation Error Estimator and the Output Error Estimator, through the simulation of modal data obtained from a computer structural analysis program and comparisons of

their results are presented so that future researchers are better informed about the two and therefore can decide which one would give the best results for their application.

DEDICATION

I would like to dedicate this work to my parents, for their love, advice and unconditional support through all my life, if it had not been for them, I would not be the man I am today.

To my brothers, who have taught me that it is through hard work that we can achieve anything we set our minds to.

To my grandparents, uncles, aunts, cousins, my friends in Mexico and my friends here in the US, who have been involved in all the aspects of my life and who have shared many good experiences with me.

"But by the grace of God I am what I am, and his grace which was bestowed upon me was not in vain. But I labored more abundantly than they all, yet not I, but the grace of God which was with me." 1 Corinthians 15:10

ACKNOWLEDGMENTS

I would like to thank the National Council of Science and Technology (CONACYT) for giving me the opportunity to pursue a master's degree here in the US, by providing me with a scholarship.

I also thank my advisor, Dr. Keith Hjelmstad, for his patience and guidance through the early stages of this study, and for his eagerness to teach me the concepts I did not understand at the time when I was just one his students in the Stress Analysis and Structural Dynamics classes.

Finally, I thank the members of my committee Dr. Subramaniam Rajan and Dr. Apostolos Fafitis, for taking the time in their busy schedules to be a part of this work, and also for the many lessons learned while they were my professors at ASU.

TABLE OF CONTENTS

Page

CHAPTER Page

CHAPTER Page

LIST OF TABLES

Table Page

Table Page

Table Page

LIST OF FIGURES

Figure Page

Figure Page

Figure Page

Figure Page

1. INTRODUCTION

As more and more stadia structures nowadays are being built by making use of new high strength building materials which tend to be lighter than the “old” ones, composite systems and also the fact that engineers, contractors and clients want their structures as optimized as possible, in terms of minimal materials used, there is an inevitable side effect that comes with this. The result is that structures are more flexible, and thus they become susceptible to undergone vibration problems due to the action of dynamic loading.

Furthermore, vibration problems in stadia are becoming more prominent as sport stadia become more multifunctional. Pop/rock concerts, exhibitions, boxing matches, and so forth are staged to supplement the football/sport seasons. Consequently, stadia structures must resist not only static loading, but also dynamic loading, such as machinery or heavy equipment in operation, ambient loading (wind, traffic, earthquakes) and/or human induced loads from various activities of the spectators which include, standing, jumping, stamping, clapping and dancing, particularly in response to touchdowns (in football matches) or musical beats (during concerts). These movements increase the likelihood of vibration problems in the stadia structures since the synchronized crowd movement may excite the natural frequencies of the structures causing their resonance (Reynolds et al. 2004).

Parameter estimation and system identification in mechanical sciences and structural engineering have become increasingly important areas of research in the last three decades. Identification methods have been used to establish mathematical models or to improve existing models (Banan and Hjelmstad, 1993). Many nondestructive testing methods are based on the concepts of system identification and parameter

estimation. Identification has been used for structural monitoring of load carrying systems such as aircraft, space structures, buildings, bridges, offshore platforms, and mechanical systems (Cawley 1985; Chen and Garba 1987; Stubbs, *et al.* 1989; Natke 1989; Hajela and Soeiro 1990). In offshore structures, attempts have been made to assess structural damage from changes in the frequency spectrum of the structure to ambient excitations (Vandiver 1975; Duggan, et al. 1980; Kenley and Dodds 1980). Engineers have been attracted to such methods because of the extreme difficulty and expense of under-water inspection. The aerospace and automotive industries extensively use identification techniques to verify or improve mathematical models for subsequent use in simulation, design, and control studies (Thoren 1972; Collins, *et al.* 1974; Sheena, *et al. 1982;* Flannelly and Berman 1983; Hashemi-Kia 1988; Kammer, *et al.* 1988; Stubbs, *et al.* 1989; Jiang, *et al. 1990;* Holkamp and Batill 1991).

System identification is defined by Zadeh (1962) as "the determination on the basis of input and output, of a system within a specified class of systems, to which the system under test is equivalent." Equivalence is defined by an error or loss that is a function of the process and the model input and output. If the value of the loss function is the same for two models, then they are equivalent (Banan and Hjelmstad, 1993). Parameter estimation is defined as the determination of values of the parameters that govern the behavior of the model, assuming that the structure of the model is known (Eykhoff 1974).

System identification is used to model existing structures (Hart and Yao 1977; Torkamani and Ahmadi 1988), assess structural changes in buildings after earthquakes (Distefano and Pena-Pardo 1975 and 1976; Beck 1982; DiPasquale and Cakmak 1990), evaluate seismic vulnerability of existing buildings (Ho and Aktan 1989; Aktan and Ho 1990), and identify critical collapse mechanisms of structures (Ellis, *et al.* 1990).

Parameter estimation has been used to evaluate performance of bridges from ambient, earthquake, and force transient responses (Douglas and Reid 1982; Flesch and Kernbichler 1988; Werner 1989; Raghavendrachar, *et al.* 1991). Another area of application for identification techniques is the condition monitoring of machines to enhance the efficiency of their maintenance and operation (Zimoch 1987; Tustin and Mercado 1985; Foster and Mottershead 1990; Mottershead 1990). Mathematical models have been derived to describe the mechanical behavior of composite materials (Hashin 1983; Zhang and Evans 1988; Courage, *et al.* 1990; Soeiro and Hajela 1990). These models try to deal with characteristic mechanical behavior including anisotropy, viscoelasticity, and deterioration phenomena like debonding or delamination.

1.1 Objectives

The main objectives of this thesis are as follows:

- Better understand the effect people jumping and/or dancing in synchronization has on the response of the TCF Bank Stadium.
- Implement models that capture the behavior of the passive people present as well as to determine how the location of standing or seated humans affect the response of a structure, whether they increase or decrease the response, in terms of displacements, accelerations, shear force or bending moment.
- Comparison between two parameter estimation algorithms from modal data in order to determine which one would give the best results, analyzing as well the effect of quantity of measurements, through incompleteness of data, and the quality of measurements, through noise modeling.

1.2 Organization

Chapter 2 provides with enough background information on the human-structure interaction problem, discussing the models developed in the past for active and passive people. In addition the fundamentals for the parameter estimation algorithms is presented, as well as the two methods that will be used in this study.

Chapter 3 presents the information that was required in order to create the finite element models of the test subjects, particularly, a three span beam (TSB) supported by four spring supports and the model for the TCF Bank Stadium.

Chapter 4 is devoted to the results obtained from static and dynamic analyses on the test structures, implementing the concepts of the human-structure interaction problem discussed in chapter 2. Comparisons between the static and dynamic analyses are presented as well as the differences that arise by considering passive people alongside active people in the structure.

Chapter 5 discusses the results obtained after running the parameter estimation algorithms for both the TSB and the TCF Bank Stadium, by analyzing the statistical indices, which are the normal check for this methods in order to see if they provide good results, and the estimated parameters.

Chapter 6 provides a detail conclusion of the analyses that were carried out in terms of the human-structure interaction problem and in terms of the parameter estimation algorithms.

2. LITERATURE REVIEW

2.1 Background and overview

Excessive vibrations can sometimes produce damage to a structure, one example of this is the accident that happened on April 25, 2008 where a part of a grandstand in the Guillermo Plazas Alcid Stadium in Neiva, Colombia collapsed during a musical event killing one person and injuring three more (Ortiz et al. 2009), thus complete and accurate structural analysis of a structure that is exposed to the dynamic loadings produced by people jumping/dancing in a synchronized fashion must be performed in order to determine the level of stresses in critical elements of the structure. Vibrations can also cause annoyance and discomfort in which case serviceability checks would have to be strictly followed to determine whether or not a structure is suitable for a certain type/level of dynamic excitation.

Most of the times these vibrations occur in structures that have a low stiffness value and correspondingly a low value of the dominant natural frequency and also in structures that have low damping. In modern stadia structures, aesthetical demands and the requirement for an unobstructed view for spectators, combined with the fact that the capacity of a stadium has to be maximized to ensure business profitability, have resulted in the design of lighter and more slender structures, often including long cantilevers. These structures often have relatively low natural frequencies that can lead to vibration problems (Reynolds et al. 2004).

2.2 Human-Structure interaction fundamentals

The presence of spectators in stadia structures can be clearly divided into two: active and passive crowds (Sim, 2006). It has been reported in (Ellis et al. 2000), that a

passive or stationary crowd will interact with the structure, whereas an active or jumping crowd will act solely as a load. Next are presented some of the theoretical background that will be needed in order to properly model both the active and passive crowds in the TCF Bank Stadium structure.

2.2.1 Active models for people

If we want to analyze the response of any structure to a particular loading type, in this case human-induced loads, we need to know what loads will act on the structure. This requires an estimation of the number and weight of people who will be jumping/dancing in the area of concern, or the load density. Also, there are many different types of dancing and a wide range of beat frequencies for music; however, dancing frequencies tend to be in the range 1.5-3.5 Hz (Ellis and Ji, 1994).

There are a number of different dances but, for analytical purposes, it is convenient to split them into two categories. The first is when the dancer is always in contact with the floor and the second involves jumping when contact with the floor is not maintained. The first type of dancing is simple to model and is primarily a sinusoidal load at the dance frequency (Supplement to the NBC, 1985). The second type of dancing is more complex and potentially much more severe because energy is input at the dance frequency and also at multiples of the dance frequency (Ellis and Ji, 1994). Throughout the rest of this work, attention will be given to the second type of loading since the effect that it could have on the structure is more severe than the first type of load mentioned.

There are two load models that will be discussed in this section. Both of them have close forms of the sum of an infinite trigonometric series and it is also illustrated in (Duarte and Ji, 2009) and (Parkhouse and Ewins, 2006) that using the first few terms is enough in practice.

The first model assumes that the load time history of the jump/dance can be described by a high contact force for a certain time t_p (contact duration) followed by zero force when the feet leave the floor. The function given in (Bachmann and Ammann, 1987) within one period is:

$$F(t)=\begin{cases} K_p G \sin(\pi t / t_p) & 0 \le t \le t_p \\ 0 & t_p \le t \le T_p \end{cases} \tag{2.1}$$

where,

K_p is F_{max}/G, impact factor

F_{max} is the peak dynamic load

G is the weight of dancers

t_p is the contact duration

T_p is the period of dancing load

The contact duration t_p can vary from 0 to T_p, corresponding to different movements and activities. The contact ratio α is defined as follows:

$$\alpha = \frac{t_p}{T_p} \le 1.0 \tag{2.2}$$

Thus different contact ratios α characterize different rhythmic activities. For analysis purposes, it is useful to express Eqn. (2.1) in terms of Fourier series as

$$F(t) = G\left(a_0 + \sum_{n=1}^{\infty} a_n \cos\frac{2n\pi}{T_p} t + \sum_{n=1}^{\infty} b_n \sin\frac{2n\pi}{T_p} t \right) = G\left[a_0 + \sum_{n=1}^{\infty} r_n \sin\left(\frac{2n\pi}{T_p} t + \phi_n \right) \right] \tag{2.3}$$

Where the Fourier coefficients and phase lags are determined as follows:

$$a_0 = \frac{2K_p\alpha}{\pi} \tag{2.4}$$

$$r_n = \sqrt{a_n^2 + b_n^2} \tag{2.5}$$

$$\phi_n = \tan^{-1}\left(\frac{a_n}{b_n}\right) \tag{2.6}$$

When $2n\alpha = 1$ for $n = 1, 2, 3,...$

Then $a_n = 0$ $b_n = \alpha K_p$

Otherwise

$$a_n = \frac{K_p\alpha}{\pi}\left[\frac{\cos(2n\alpha - 1)\pi - 1}{2n\alpha - 1} - \frac{\cos(2n\alpha + 1)\pi - 1}{2n\alpha + 1}\right] \tag{2.7}$$

$$b_n = \frac{K_p\alpha}{\pi}\left[\frac{\sin(2n\alpha - 1)\pi}{2n\alpha - 1} - \frac{\sin(2n\alpha + 1)\pi}{2n\alpha + 1}\right] \tag{2.8}$$

It was experimentally observed in (Tuan and Saul, 1985) that the mean value of the time history of a vertical load corresponding to rhythmic jumping was always equal to the weight of the performer. This was later confirmed in (Ellis and Ji[2], 1994). Expressing this observation analytically gives

$$\frac{1}{T_p}\int_0^{t_p} K_p G \sin\left(\frac{\pi t}{t_p}\right) dt = G \tag{2.9}$$

Which reduces to

$$K_p = \frac{\pi}{2\alpha} \tag{2.10}$$

Thus the loads can be determined knowing the weight of the jumper, the period of the jumping and the contact ratio.

Substituting Eqn. (2.10) into Eqn. (2.3) yields

$$F(t) = G\left(1.0 + \sum_{n=1}^{\infty} a_n \cos\frac{2n\pi}{T_p}t + \sum_{n=1}^{\infty} b_n \sin\frac{2n\pi}{T_p}t\right) = G\left[1.0 + \sum_{n=1}^{\infty} r_n \sin\left(\frac{2n\pi}{T_p}t + \phi_n\right)\right] \tag{2.11}$$

$$r_n = \sqrt{a_n^2 + b_n^2} \qquad \phi_n = \tan^{-1}\left(\frac{a_n}{b_n}\right)$$

When $2n\alpha = 1$ for $n = 1, 2, 3,\ldots$

Then $a_n = 0$ $b_n = \pi/2$

Otherwise

$$a_n = 0.5\left[\frac{\cos(2n\alpha - 1)\pi - 1}{2n\alpha - 1} - \frac{\cos(2n\alpha + 1)\pi - 1}{2n\alpha + 1}\right]$$

$$b_n = 0.5\left[\frac{\sin(2n\alpha - 1)\pi}{2n\alpha - 1} - \frac{\sin(2n\alpha + 1)\pi}{2n\alpha + 1}\right] \tag{2.12}$$

The second model is based on the jumping and bobbing experiment carried out in the University of Surrey, Parkhouse and Ewins (2006) have given the bouncing load in a Fourier series form as shown in Eqn. 2.13. All measurements were made on an area, 0.8 m by 0.6 m, consisting of two AMTI BP400600MF-2000 force platforms (Sumit Medical and Scientific, UK) rigidly fixed with the floor.

$$F(t) = G\left[1.0 + \sum_{n=1}^{\infty} r_n \cos\left(2n\pi f_p t - \phi_n\right)\right] \tag{2.13}$$

Where f_p is the frequency of the dancing/jumping load, r_n and φ_n are both derived from the mean of the bouncing load time history from the statistical analysis of selected groups.

Considering both the reliability and the convenience for calculation, it was concluded by Yang (2010) that the first model presented in equations 2.11 and 2.12 is recommended for use, however, it may also need some adjustments from practice because of its indoor test limitations, such as most of their tests carried out on simply supported reinforced concrete beams and the omission of group effect analysis.

2.2.1.1 Frequency range for active people

Ellis and Ji (2004) suggested that the frequency range for individuals jumping is approximately 1.5-3.5 Hz, but for a crowd the higher-frequency jumping cannot be sustained and an upper limit of 2.8 Hz is more realistic. However, it was recognized that further detailed information was required, examining the actual range at which people can jump comfortably and where a crowd can achieve some degree of coordination.
To investigate the frequency range, the beat frequencies of a sample of 210 modern popular songs were examined in (Ginty et al. 2001). The investigation included tests to assess the frequency ranges for coordinated dance-type loads for individuals, small groups (aerobics) and large groups (pop concerts). Some of the conclusions from this work were that the frequency ranges are:

(a) 1.2-2.8 Hz for an individual jumping.

(b) 1.5-2.5 Hz for a small group jumping (aerobics) with some degree of coordination.

(c) 1.8-2.3 Hz for a large group jumping (pop concerts) with some degree of coordination.

For the purpose of this study the frequency range between 1.8 and 2.3 Hz will be used, since the number of people that can be present in the section of the stadium could be considered as large (more than 3,000 people).

2.2.1.2 Dynamic crowd effect

In the previous section, the derivation to compute the load produced by one person jumping was presented, however, when performing and analysis of a stadium structure or part of the stadium there are more than one people jumping/dancing to the beat of a particular song, therefore the actual load density and distribution of the crowd should also be considered. Consideration should also be given to the dynamic crowd effect, which describes the attenuation of load due to the imperfect coordination between individuals in a group.

Although, it has been found that dynamic loads induced by groups of people are higher than those induced by individuals, the human-induced forces do not increase linearly with the number of people (Sache et al., 2002). This is so even if people are synchronized by a prompt (Ebrahimpour and Sack, 1992; Kasperski and Niemann, 1993) that can be provided by music, movements of other people, or perceptible movements of the occupied structure (Fujino et al. 1993; van Staalduinen and Courage, 1994).

The dynamic crowd effect depends on the coordination of the people in the group, the type of dancing and the beat frequency of the music. A theoretical investigation

where the phase lag between individuals was treated as a random variable obeying a normal distribution, showed a one-third reduction of the crowd loads for a large group of people (Ji and Ellis, 1993). Furthermore, Annex A of the BS 6399-1:1996, specifies that a factor of 0.67 should be included when computing the load induced by a crowd of people jumping/dancing at a specific musical beat so that the effect of lack of synchronization can be taken into consideration.

Considering the information presented in this section, the model that will be used throughout the rest of this work is the one presented in the set of equations 2.11 and 2.12, along with the synchronization factor of 0.67.

2.2.2 Passive models for people

Ellis et al. (2000) performed an experiment on a cantilever grandstand where a stationary crowd was present. They monitored the grandstand before and after a rugby match, mainly the vertical response of a cantilever section. They suggested that the stationary or passive crowd acts as a spring-mass system, in addition to the fact that passive crowd provides a significant increase in the damping of the entire system. Littler (2000) presented a similar experiment that was performed in a retractable grandstand. The results showed the inadequacy of representing a passive crowd just as an added mass. Reynolds et al. (2004), Sachse et al. (2002), Ellis and Ji (1997) and Sachse (2002) also agree that a crowd-occupied structure should be modelled as a dynamic system.

In order to determine mathematically the influence of the passive crowd, whether they are standing or seating, on stadia structures or any other structure, there are a limited number of dynamic models of human occupants. These models can be divided

into damped and undamped models (Sache et al., 2003). In this section the damped models are presented.

2.2.2.1 Damped models

Biomechanical research established that the human body is heavily damped. This was recognized by civil engineers and led to the development and use of some damped SDOF models of human occupants (Figures 1, 2 and 3).

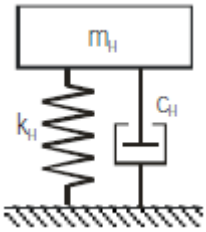

Figure 1. SDOF Human whole-body model

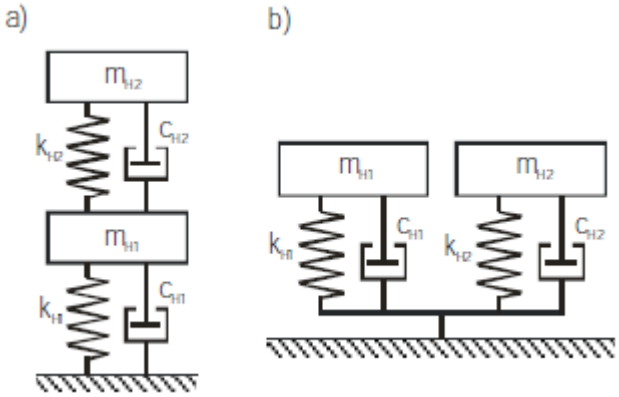

Figure 2. 2-DOF (a) and 2-SDOF (b) human whole-body model

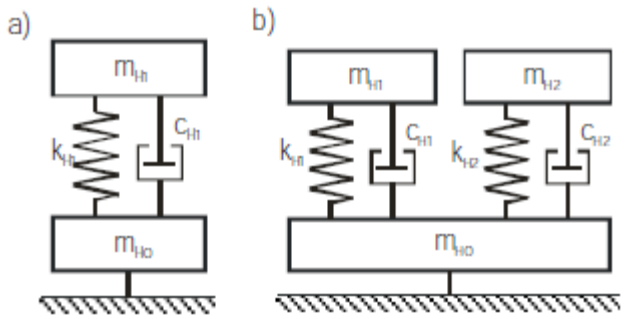

Figure 3. SDOF (a) and 2-SDOF (b) human whole-body model with a non-vibrating mass

Foschi and Gupta (1987) were the first to use a damped dynamic human model. This was done to predict the vibration response of wooden floors to heel-drop excitation. This, and subsequent research by Folz and Foschi (1991) and Foschi et al. (1995) into response time histories to assess the serviceability of floors led to damped SDOF models characterized by an assumed lumped mass m_H equal to the total mass m_T of the impactor, a viscous dashpot c_H = 1.25 kNs/m and a stiffness k_H = 40 kN/m (Foschi et al., 1995).

Falati (1999) added a viscous dashpot to his undamped SDOF model (f_H = 10.43 Hz, $m_H = m_T/3$) presented earlier and thus developed a damped SDOF model (Figure 1) of a standing (not impacting) person (Table 1). To determine the damping ratio of the damped SDOF human model, Falati computed responses of the structural DOF of damped 2-DOF human-structure models and compared them to experimental time histories. He identified the damping ratio to be within a range from 45% to 55% and employed the median value of 50% to define a model of a standing person (Table 1).

Another damped SDOF model of a human occupant was used by Brownjohn (1999) to predict the influence of a standing human occupant on his test structure. For this purpose, he defined a damped SDOF model assuming the lumped mass m_H to be the

total mass m_T of the human occupant (Table 1). Brownjohn also choose the stiffness k_H and the viscous damping c_H to lead to a natural frequency f_H and a damping ratio ζ_H corresponding to the fundamental mode of a 4-DOF human model given by ISO 7962 (ISO, 1987).

Table 1. Characteristics of damped SDOF models of a standing human occupant

Human Model	Spatial properties	Modal properties
Falati (1999)	$m_H = m_T/3$ (25 kg)	f_H = 10.43 Hz ζ_H = 50%
	k_H = 107 kN/m	
	c_H = 1.636 kNs/m	
Brownjohn (1999)	$m_H = m_T$ (80 kg)	f_H = 4.9 Hz ζ_H = 37%
	k_H = 82 kN/m	
	c_H = 1.946 kNs/m	

Brownjohn (2001) fitted a damped SDOF model into the apparent mass of a single person with a total mass of 47 kg standing on a test structure. He obtained the best SDOF circle-fit for f_H= 5.8 Hz, ζ_H = 38% and a lumped mass m_H = 60 kg, thus exceeding the weight of the occupant. Thus, Brownjohn found the natural frequency f_H of a SDOF model of a single standing person to be significantly higher than the 4.9 Hz of his first human model (Brownjohn, 1999).

To determine the variability of the natural frequencies of standing humans, Zheng and Brownjohn (2001) estimated natural frequencies f_H of 30 standing individuals. For this purpose, they used a 4 m long reinforced simply-supported concrete plank that had a fundamental natural frequency of 12.8 Hz. Zheng and Brownjohn (2001) estimated natural frequencies and damping ratios of the empty structure and of the structure with each of the 30 test subjects standing at midspan.

Zheng and Brownjohn (2001) used these experimental natural frequencies and damping ratios to compute the natural frequencies f_H and the damping ratios ζ_H of damped SDOF models of individual occupants. This calculation also used the modal mass of the fundamental mode of the empty structure, which was probably calculated from the spatial properties of the structure. Additionally, it required the lumped mass of the SDOF occupant model to be known. Similar to most other researchers, Zheng and Brownjohn (2001) set this mass m_H to be equal to the total mass of the occupant.

Zheng and Brownjohn (2001) concluded that f_H and ζ_H of the test subjects are about 5.24 Hz and 39%, respectively. Thus, the identified natural frequencies f_H match biomechanical research (Tables 2 and 3) more closely than the significantly higher identified by Ji (1995) and Falati (1999). However, Zheng and Brownjohn (2001) found no clear dependency of f_H on the total mass m_T, the height, or the mass/height ratio of individuals.

Table 2. Characteristics of biomechanical models of a sitting human subjected to vertical vibrations. Imperial units were converted into metric units employing Beranek (1988: appendix B3)

a) Based on the mechanical impedances of 8 men.
b) Based on the mechanical impedances of 11 men.
c) Based on the apparent masses of 60 people.

Model	Spatial properties	Modal properties
Coermann (1962) [a] Damped SDOF model	m_H = 86.2 kg (86200 dyne s^2/cm)	f_1 = 5.0 Hz
	k_H = 85.25 kN/m (85.25 dyne/cm)	ζ_1 = 32%
	c_H = 1.72 kNs/m (1.72X10^6 dyne s/cm)	
Suggs et al. (1969) [b] 2-SDOF model	m_{H1} = 36.3 kg (80 lb)	f_1 = 4.5 Hz
	k_{H1} = 28.45 kN/m (1952 lb/ft)	ζ_1 = 23%
	c_{H1} = 474 Ns/m (32.5 lb s/ft)	
	m_{H2} = 12.5 kg (27.6 lb)	f_2 = 5.5 Hz
	k_{H2} = 15.03 kN/m (1030 lb/ft)	ζ_2 = 31%
	c_{H2} = 271 Ns/m (18.6 lb s/ft)	
Wei and Griffin (1998) [c] 2-SDOF model with non-vibrating mass	m_{H0} = 4.1 kg	-
	m_{H1} = 46.7 kg	f_1 = 4.9 Hz
	k_{H1} = 44.115 kN/m	ζ_1 = 53%
	c_{H1} = 1.522 kNs/m	
Wei and Griffin (1998) [c] 2-SDOF model with non-vibrating mass	m_{H0} = 5.6 kg	-
	m_{H1} = 36.2 kg	f_1 = 4.9 Hz
	k_{H1} = 35.007 kN/m	ζ_1 = 36%
	c_{H1} = 815 Ns/m	
	m_{H2} = 8.9 kg	f2 = 9.7 Hz
	k_{H2} = 33.254 kN/m	ζ_2 = 44%
	c_{H2} = 484 Ns/m	

Table 3. Characteristics of human models specified in ISO 5982 (ISO, 1981)

Model	Spatial properties	Modal properties
ISO 5982 (ISO 1981): 2-SDOF model of the seated human body	m_{H1} = 69 kg	f_1 = 5.0 Hz
	k_{H1} = 68 kN/m	ζ_1 = 36%
	c_{H1} = 1.54 kNs/m	
	m_{H2} = 6 kg	f_2 = 10.1 Hz
	k_{H2} = 24 kN/m	ζ_2 = 25%
	c_{H2} = 0.19 kNs/m	
ISO 5982 (ISO 1981): 2-SDOF model of the standing human body	m_{H1} = 62 kg	f_1 = 5.0 Hz
	k_{H1} = 62 kN/m	ζ_1 = 37%
	c_{H1} = 1.46 kNs/m	
	m_{H2} = 13 kg	f_2 = 12.5 Hz
	k_{H2} = 80 kN/m	ζ_2 = 46%
	c_{H2} = 0.93 kNs/m	

2.2.3 Analysis of the human-structure interaction problem

In order to analyze a structure subjected to human loading, more specifically jumping and/or dancing loads, it is convenient to treat the active people as just load, whereas the passive people should be considered as a spring-mass-damper system as reported by Ellis et al. (2000). This can be better described by looking at figure 4.

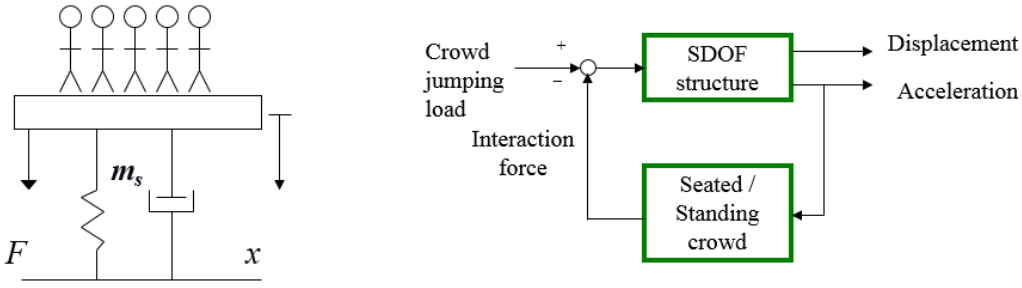

Figure 4. Passive crowd-SDOF system subjected to crowd jumping load and a corresponding feedback system representation

2.3 Serviceability assessment after dynamic analysis

For serviceability assessments related to human perception of vibrations, it is the acceleration levels which must be determined. However, the question of what are acceptable vibration levels must then be considered (Ellis and Littler, 2000).

For guidance on acceptable vibration levels in grandstands subject to jumping loads, it seems appropriate to examine data obtained at such events. A number of experiments have been undertaken in Germany, (Kasperski M., 1996), and recommendations for low-frequency vibration are given in Table 4.

Table 4. Reaction of people to various acceleration levels on grandstands

Vibration level	Reaction
< 5% g	Reasonable limit for passive persons
< 18% g	Disturbing
< 35% g	Unacceptable
> 35% g	Probably causing panic

2.4 Parameter estimation problem from modal data

2.4.1 Introduction

Very few structural systems can be adequately modeled using theory alone; there are always parameters in an analytical model, particularly constitutive parameters, whose values must be assumed or empirically determined. Physical testing of a structure often provides valuable information that a theory cannot provide. However, test data are often incomprehensible without a theoretical framework to aid the data reduction. System identification and parameter estimation are the natural tools for bridging the gap between an analytical model and test data (Banan and Hjelmstad, 1993).

To build a mathematical model we begin with generally accepted physical laws. In structural mechanics these laws include balance of linear and angular momentum, kinematics of deformation, and the constitutive behavior of materials. The governing equations, based upon those things that we know well, provide the structure for our identification model. The aspects of the model that we do not know are parameterized and left to be estimated from the data. In a test we seek to excite the structure in a manner that will encourage a mode of response that will help the most in identifying the parameters of the model. In addition, we try to measure those quantities that are most indicative of the structural characteristics. It is often important to make those measurements as accurate as possible (Banan and Hjelmstad, 1993).

Further, it is assumed that the structure is amenable to discretization using the finite element method. Even though we know that, in general, a real structural system will behave nonlinearly, one can often justify such a limitation by observing that a linear model is the first order approximation of any nonlinear system and that most structures respond linearly over some reasonably interesting range of excitation (Banan and Hjelmstad, 1993).

One of the greatest challenges in performing a test on a large structural system lies in exciting the structure. A modal dynamic test relies on resonant excitation of the structure. The dynamic magnification at resonance for lightly damped structures is easily accomplished with a modest force. Such a force might be generated by rotating an eccentric mass at a fixed resonant frequency. Many modes can be excited by resonance, provided the integrity of the connection between the structure and the exciting device is not compromised by the motion. Some modal tests use free vibration data, generated, for example by imparting an initial displacement or an initial velocity to the structure.

Imparting an initial displacement is easily done in a laboratory, but may be impossible in the field. Imparting an initial velocity can be accomplished using falling weights or by impulsive forces generated by explosive cartridges or small rockets. For most structures, only the lowest few modes of vibration can be excited in free vibration (Banan and Hjelmstad, 1993).

The process of system identification consists of three main stages (Banan and Hjelmstad, 1993); (1) defining a model and arranging some experiments to measure the response of the system (model selection), (2) using the chosen model and the measured response to estimate the unknown parameters of the model (parameter estimation), and finally (3) validating and refining the model if necessary (diagnostic check).

A model is a representation of the essential aspects of a system that contains knowledge of that system in a usable form (Eykhoff 1974). Model selection is basically governed by three choices (Banan and Hjelmstad, 1993): (1) the candidate class of models, (2) the structure and size of the chosen model, and (3) parameterization of the chosen model. The intended use of the model usually dictates the class of the model. Choosing the size of the model is not a trivial problem because the model is often a representation of an unknown process. The model should include only the essential features of the real system to avoid introducing unnecessary complication. The parameterization of the model should be guided by three important objectives (Niederlinski and Hajdasinski 1979): (1) the parameterization should be universal, *i.e.* the model should be applicable to all systems in the same class, (2) the number of parameters should be in accord with the limited information available, and (3) the model should be identifiable from the available information.

The main goal of designing an experiment is to provide maximum information about the parameters of the system to be identified. There are many factors involving in the design of an experiment. These include the intended application of the results, prior knowledge about the system, the structure of the model, the measure of equivalence to the real system, the parameter estimation method, and the operational constraints of the system (Banan and Hjelmstad, 1993).

The essence of building a model for a real system is its capability to simulate and/or to predict the behavior of the system. The performance of the model can be evaluated by a loss function that indicates how well the model fulfills the intended tasks. It is natural to minimize the discrepancy between the model and the system by tuning the parameters of the model. The essence of parameter estimation is to find parameters which minimize a scalar measure of discrepancy known as the criterion of equivalency or loss function. A procedure for estimating parameters is referred to as a parameter *estimator* (Banan and Hjelmstad, 1993). In the statistical literature, a number of different estimators have been developed. These methods differ predominantly in the criterion of equivalency and in the use of available prior information about the statistics of the measurements and the parameters.

There are two basic approaches for estimating the parameters: the *off-line* or *batch* method and the *on-line* or *recursive* method. In the batch approach the computational operations are carried out on the complete set of measurements as a whole. Another way of processing the measurements is to continuously update the estimation of parameters while working serially through the measurements. The recursive approach generates an updated estimation as it receives new information. The batch method is computationally more efficient and robust than the recursive method.

However, recursive methods are popular in the field of control and automation because they do not require the storage of raw data.

A model obtained from the identification process has to be validated to ensure that it describes the system suitably for its intended application (Banan and Hjelmstad, 1993). Model testing is the most difficult phase of the identification process and can be very subjective. In general, there are two approaches to examine the identified model. Compare the results of the model with the results of the best models from the other classes of models, or decide whether the properties of the model meet some reasonable requirements such as cross-validation, residuals, and consistency with *a priori* knowledge not used in the estimation. Model validation is subjective and, regardless of the validation criteria, one must judge for one's self to what extend the model really explains the behavior of the system (Banan and Hjelmstad, 1993).

2.4.2 Parameter estimation algorithms

In undamped free vibration a structure responds in modes governed by the following discrete eigenvalue problem

$$K(x)u_i = \lambda_i M u_i \qquad i = 1,\ldots,nmd \tag{2.14}$$

Where *nmd* is the number of measured modes, the eigenvalue λ_i is the square of the ith angular frequency, $u_i(n_d \text{ x } 1)$ is the ith mode shape (eigenvector), $K(n_d \text{ x } n_d)$ is the stiffness matrix, *x* is the vector of unknown constitutive parameters with dimension *np, matrix* $M(n_d \text{ x } n_d)$ is the mass matrix, and n_d is the number of degrees of freedom. The eigenvalue problem has n_d eigenpairs (λ, u) for a positive definite M and a positive semi-definite *K* matrix. One will generally not have a complete set of measured eigenpairs (λ_i, u_i), but rather a subset of them numbering $nmd<n_d$, which might not contain all the

modes between the largest and the smallest measured frequencies. It is assumed that the mass matrix is completely known and only the stiffness parameters of the structure need to be estimated.

One of the main difficulties in estimating the unknown parameters from modal data is that the mode shapes u_i are often sparsely sampled in space. There are several reasons why sparsity of measurement locations is not exceptional. First, there may be regions of the structure that are inaccessible because they lie on the interior of a solid domain. Second, certain types of measurements may be impractical to make because of technological limitations, *e.g*. nodal rotations. Third, the number of sensors may be limited due to their cost. Even if one measures displacements at all of the degrees of freedom of a model, these measurements become sparse if we subdivide the mesh of the model.

To overcome the problem of incomplete measurements, Banan and Hjelmstad (1993) partitioned the mode shape vector into two parts as follows

$$u_i = \begin{bmatrix} \hat{u}_i \\ \bar{u}_i \end{bmatrix} \equiv u_i(\bar{u}_i) \tag{2.15}$$

Where $\hat{u}_i\left(\hat{n}_d x1\right)$ and $\bar{u}_i\left(\bar{n}_d x1\right)$ are the vectors of measured and unmeasured modal displacements, respectively and $\hat{n}_d$ and $\bar{n}_d$ are the number of measured and unmeasured degrees of freedom, respectively. The notation indicates that the total displacement vector u is a function of the unknown displacements. For practical purposes it is assumed that this partitioning is fixed for all measured modes.

The discrete governing equation of the finite element model of a structure for undamped free vibration is given in Eqn. (2.14) which is refer to as the model equation.

Now, the known mass matrix of the model is partitioned into two matrices: a matrix corresponding to the measured displacements $\hat{M}\left(n_d x \hat{n}_d\right)$ and a matrix corresponding to the unmeasured displacements $\overline{M}\left(n_d x \overline{n}_d\right)$ and rewrite Eqn. (2.14) based on the partition in Eqn. (2.15) as follows

$$K(x)u_i = \lambda_i \left[\hat{M} \quad 0\right] u_i + \lambda_i \left[0 \quad \overline{M}\right] u_i \qquad i = 1,\ldots,nmd \tag{2.16}$$

In the right hand side of Eqn. (2.16) the first term is a completely known vector and the second term contains the unknown vector $\overline{u}_i$. Now, arranging Eqn. (2.16) we have

$$\left[K(x) - \lambda_i \left[0 \quad \overline{M}\right]\right] u_i = \lambda_i \left[\hat{M} \quad 0\right] u_i \tag{2.17}$$

And define a modified stiffness matrix $K_i^*(x)$ and a force vector f_i^* as follows

$$K_i^*(x) = K(x) - \lambda_i \left[0 \quad \overline{M}\right] \tag{2.18}$$

$$f_i^* = \lambda_i \left[\hat{M} \quad 0\right] u_i$$

By substituting equations (2.18) into Eqn. (2.17) the modified model equation becomes (Banan and Hjelmstad, 1993)

$$K_i^*(x) u_i = f_i^* \qquad i = 1,\ldots,nmd \tag{2.19}$$

Which is almost the same as the governing equation of a structure under *nmd* static load cases. The only difference between the modified model equation and a static equilibrium equation is in the definition of the stiffness matrix. In Eqn. (2.19) the modified stiffness matrix is a function of the eigenvalues, changing for each mode. The

stiffness matrix for a static problem is fixed for all load cases. All the operations used to derive Eqn. (2.19) from Eqn. (2.14) are reversible. If one finds a set of parameters *x* that satisfies the modified model Eqn. (2.19), these parameters also satisfy the eigenvalue problem (2.14). From now on Eqn. (2.19) is referred to as the model equation for an undamped free-vibration experiment.

Consider a structure (sometime referred to as the *real structure* even though a simulation model will be used) subjected to *N* different excitation cases and the response at certain locations has been observed. Where *N* will be the number of *observation sets:* The number of measured modes for the free vibration problem. A finite element model of the subject structure is available, parameterized by certain constitutive properties. The unknown parameters of the finite element model are estimated by minimizing a scalar loss function *J* subject to a set of constraints, where the loss function indicates how well the model equation is satisfied. The parameter estimation problem can then be expressed as follows:

$$\min_{(x,\bar{u})} imize \qquad J(x,\bar{u}) = \frac{1}{2}\sum_{i=1}^{N} \alpha_i \left\| e_i(x,\bar{u}_i) \right\|^2 \tag{2.15}$$

$$subject\ to \qquad c(x) \le 0$$

The loss function *J* is the weighted summation of L_2 norms of the individual error functions *e* for the various observation sets. These error functions reflect the discrepancy between the estimated response of the mathematical model and the observations from the real structure, and are a function of the constitutive parameters *x* of the model as well as the unmeasured response $\bar{u}$ of the structure.

The weight α_i in Eqn. (2.15) reflects the degree of confidence to the ith set of observations. For example, in a free vibration experiment, since the lower modes are easy to measure reliably, their weights might be chosen larger than the weights for the higher modes. In a statistical sense, the best values for the weights are the inverse of the variance of the error functions.

The constraints *c(x)* are used to enforce *a priori* knowledge of the parameters. The bounding constraints are the ones that are used for most problems for the unknown constitutive parameters,

$$\underline{x} \leq x \leq \overline{x} \tag{2.16}$$

Where $\underline{x}$ and $\overline{x}$ are the lower and upper bound vectors, respectively for the unknown parameters. These bounds define the feasible region and are important because they eliminate the possibility of converging to physically unreasonable solutions. For structural systems, if the constitutive, damping, and mass parameters are chosen to be the parameters of the model, the lower bound $\underline{x}$ might be chosen greater than or equal to zero because theory insists that these parameters be positive. The upper bound $\overline{x}$ is more difficult to select, but might, for example, be chosen in the neighborhood of the nominal design values.

In order to solve the nonlinear constrained optimization problem described in Eqn. (2.15), the Matlab® Optimization Toolbox was employed using the Sequential Quadratic Programming (SQP). Appendix A present the basic theory behind the algorithm.

2.4.2.1 Equation Error Estimator (EEE)

Banan and Hjelmstad (1993) proposed this method, where they defined an error function e_i based on the residual force vector for mode i as follows

$$e_i(x,\bar{u}_i) = K_i^*(x)u_i(\bar{u}_i) - f_i^* \qquad i = 1,\ldots,nmd \tag{2.17}$$

Where x is the vector of unknown elemental constitutive parameters. The error function represents the amount of residual developed by failure to satisfy the model equation. Let $\bar{u} = (\bar{u}_1, \bar{u}_2, \ldots, \bar{u}_{nmd})$ be the vector of unmeasured modal degrees of freedom for all measured modes. Based on the general form of the estimation problem (2.15), the nonlinear constrained optimization problem for the equation error estimator for modal parameter estimation can be stated as

$$\min_{(x,\bar{u})} imize \qquad J(x,\bar{u}) = \frac{1}{2}\sum_{i=1}^{nmd} \alpha_i \left\| K_i^*(x)u_i(\bar{u}_i) - f_i^* \right\|^2 \tag{2.18}$$

$$subject\ to \qquad \underline{x} \le x \le \bar{x}$$

Where $\underline{x}$ and $\bar{x}$ are the prescribed vectors of lower and upper bounds of the unknown constitutive parameters, respectively and α_i is the weight associated to the ith mode which reflects the degree of confidence of the ith measured mode. The estimation problem (2.18) tries to satisfy the model equation in a least squares sense. The equation error estimator simultaneously estimates the unknown constitutive parameters and the unmeasured displacements for all measured modes. By adding simple bounding constraints on the unknown constitutive parameters the possibility of converging to infeasible solutions is eliminated.

2.4.2.2 Output Error Estimator (OEE)

Banan and Hjelmstad (1993) defined an error function e to be the difference between the measured and computed mode shapes at the locations where the physical measurements are taken. They define a Boolean matrix Q such that $\hat{u}_i = Qu_i$. In other words, *Q* extracts the measured modal deformation $\hat{u}_i$ from the complete vector of modal degrees of freedom u_i . It is assumed that *Q* is the same for all modes. The error function for the output error estimator is given by the following expression

$$e_i(x) = QK_i^{*-1}(x) f_i^* - \hat{u}_i \tag{2.19}$$

The vector of unknown variables contains only the unknown constitutive parameters *x* for the output error estimator. Thus, the nonlinear constrained optimization problem for the output error estimator can be stated as

$$\min_x imize \qquad J(x) = \frac{1}{2}\sum_{i=1}^{nmd} \alpha_i \left\| QK_i^{*-1}(x) f_i^* - \hat{u}_i \right\|^2 \tag{2.20}$$

$$subject\ to \qquad \underline{x} \le x \le \bar{x}$$

Where the bound vectors $\underline{x}$ and $\bar{x}$ and the weights α_i are the same as those defined in Eqn. (2.18). The number of unknowns for the output error estimator is smaller than the number of unknowns for the equation error estimator. Consequently, the solution of the former is carried out in a space of smaller dimensional than the latter. On the other hand, the loss function of the output error estimator has a higher degree of nonlinearity than the loss function of the equation error estimator.

2.4.2.3 Initial values and identifiability criterion

The equation error estimator and the output error estimator are based on nonlinear constrained optimization problems. Like any iterative process, to solve this nonlinear problem, initial values for the unknown variables are needed. The choice of starting point is one of the important factors which control the speed of convergence of the algorithm, and one should employ any prior knowledge about the parameters.

Both of the estimators need initial values for the unknown constitutive parameters. One could use design values as a reasonable choice for the initial values of the unknown parameters. One could also use analytical methods and engineering modeling to generate initial values. In the absence of any a priori knowledge, one must guess the initial values for the unknown constitutive parameters *x*. lf for some parts of the structure parameters are known, then the known parameters x_o can be used to guess initial values x^o for the unknown parameters with the same nature.

The equation error estimator also needs initial values for the unmeasured modal displacements $\bar{u}^o$. Banan and Hjelmstad (1993) found that the best way to generate $\bar{u}^o$ is to compute the modal response from the model equation (2.19), with the modified stiffness matrix K^* constructed analytically from the known parameters x_o and initial values of the unknown parameters x^o. To wit,

$$\bar{u}_i^o = PK_i^{*-1}\left(x_o, x^o\right) f_i^* \qquad i = 1,\ldots,nmd \tag{2.21}$$

Where the matrix P is a Boolean matrix that picks the unmeasured displacements $\bar{u}_i^o$ from the total computed displacements $\bar{u}_i^o$.

Both estimators use the sequential quadratic programming (SQP) algorithm to minimize the loss function. The SQP algorithm is an iterative gradient search strategy that uses the local information about the gradient and curvature of the loss function at the current point in the space of optimization variables and computes a direction vector and a step length to reach the next point.

The estimators for modal problems are in the class of least-squares estimators, and thus cannot reliably make an estimation if less than a certain minimum amount of data are available. Confidence in the estimates increases with the amount of information above this minimum level. The basic identifiability criterion is

$$\left(nmd \times \hat{n}_d\right) \geq n_p \tag{2.22}$$

Where $\left(nmd \times \hat{n}_d\right)$ is the number of independent measurements and n_p is the number of unknown constitutive parameters. The identifiability criterion (2.22) is a quantitative index for the richness of the available information. If this criterion is not satisfied, then the estimates are totally unreliable. However, satisfaction of the identifiability criterion does not guarantee reliable estimates.

2.4.3 Simulation environment

The behavior of a parameter estimation procedure depends on two factors: the mathematical model and the richness of the data. The selection of an adequate model is difficult and often requires the intuition and judgement of an expert. The subjective step of model selection is avoided completely by simulation so that the focus can be on the problem of evaluating the issue of the richness of the data (Banan and Hjelmstad, 1993). To minimize model selection as a source of error, “real” data is generated by simulation with the model that will be used as the basis of the parameter estimation scheme (the

model created in Staad Pro). Thus, the assumed mathematical model is an exact representation of the "real" structure and is valid. The only factor affecting the behavior of the parameter estimation algorithm, then, is the richness of the measurements.

The term richness is used as a descriptor for the information content in the data. It is related not only to the quantity of measurements but also to the quality of those measurements. One compromise to the quality of the data comes from the noise *(e.g.* from experimental errors) in the measurements. Experimental errors are developed from a variety of sources. Some of the errors are systematic and some of them are random.

Whenever some aspect of a given problem has a random nature, the solution to that problem is a random variable. In a parameter estimation problem, the measurements can be considered to have a random error component, therefore the estimated parameters are random variables. The essential problem is to discover the statistical properties of the solution, in this case the statistics of the estimated parameters. Determination of the statistics of the solution is particularly difficult when the problem is nonlinear or complex (or both). Monte Carlo simulation provides a useful tool for these problems.

In the parameter estimation problem, the parameters of a finite element model are estimated, by solving the constrained nonlinear optimization problem expressed by Eqn. (2.15). For a given finite element model, set of load cases, bounding constraints, and initial values, the solution x is a function only of the response u measured at certain locations. These response values will be polluted with noise. In the simulation environment the noisy response u is generated by adding a noise vector n to the computed response of the given finite element model u_o as follows

$$u = u_o + n \tag{2.23}$$

Where n is a random vector with zero expected value and finite known variance. As schematically shown in Fig. 5, the experimental errors are modeled as a random noise vector *n* with an assumed distribution function. The response *u,* computed in accord with Fig. 5, is taken to be the measured response of the real structure.

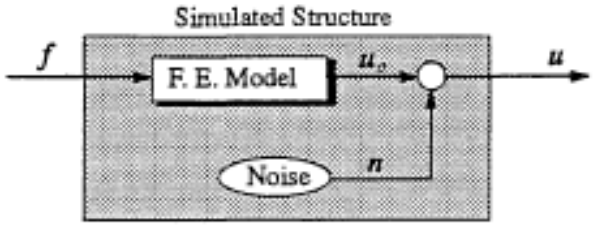

Figure 5. Simulation of actual response of the structure

The estimated parameters *x* are functions of the noisy response *u* which is a random vector. Therefore, the solution *x* becomes a random vector whose distribution directly depends on the distribution of the noise vector *n* and the mathematical characteristics of the estimation problem (2.15). Through Monte Carlo simulation a population of random solutions *x* from noisy data whose statistics are completely known can be generated. Each individual member of the solution population corresponds to a certain noise vector.

For a given mathematical model, bounding constraints, initial values, and load cases, Monte Carlo simulation uses a random number generator to produce a sequence of noisy responses as follows

$$u^t = u_o + n^t \qquad t = 1,\ldots,T \tag{2.24}$$

Where n^t is the tth noise vector computed using the random number generator as explained in the next section and T is the sample size. For each individual noisy response u^t, the parameter estimation algorithm computes an estimate of the parameters x^t of the mathematical model. Hence, the simulation develops a sample $\{x^t, t = 1,...,T\}$ of estimates (i.e. the solution population). Based on the law of large numbers, by increasing the sample size T, the statistical indices of the sample (e.g. the mean and standard deviation) converge to the actual statistics of the population. Monte Carlo simulation does not need the explicit form of the relationship among inputs and outputs of the algorithm and approximates the distribution of the estimated parameters by executing the algorithm repeatedly, each time altering only the values of the imposed noise. An individual execution of the estimator is referred to as a trial in the subsequent sections. The sample size T (number of trials) should be large enough to establish statistical significance of the estimates. The variation of the statistical indices of the sample with respect to the sample size becomes steady when the number of trials is large enough.

2.4.3.1 Noise modeling

In the simulation study, real measurements are not available, so noisy response is simulated by adding random noise to the computed response. There are many types of errors that can be introduced into a mathematical model to simulate noisy measurements. Due to the complexity of the measurement process, any single type of random error would fall short of modeling the actual error experienced in the field. Therefore, two simple types of random noise (error) are used to bound the problem of noise modeling. The first type is an absolute error of amplitude λ multiplying a uniform random variable ξ that takes values between plus and minus one. The error is added to

the computed response u_o to simulate noisy measurements. Thus, the simulated absolute measurement error is modeled as

$$u_i^t = u_{o_i} + \lambda \xi_i^t \qquad i = 1,\ldots,\hat{n}_d \qquad t = 1,\ldots,T \tag{2.25}$$

Where $\hat{n}_d$ is the number of measured degrees of freedom for a load case, and T *is* the sample size for the simulation. The random variable ξ is constructed using a pseudo-random number generator and has a zero expected value and variance equal to 1/3. Equation (2.25) shows that errors added at each measured degree of freedom for each trial ξ_i^t are independent from one another.

Absolute errors model actual experimental errors well when all instruments have the same sensitivity and are used to measure responses of the same type and order of magnitude. If some of the measurements are small, the absolute errors tend to overwhelm the actual responses. The smaller deformations may be unfairly penalized, because in practice, when the deformations are suspected to be small, the sensors would be set to a greater sensitivity. Also, if the same error amplitude is applied to measurements of different types (such as displacements and rotations) the errors can completely dominate the smaller response.

The second type of error is the proportional error. This error is a fraction of the computed response multiplying a uniform random variable ξ defined in Eqn. (2.25). The simulated proportional measurement error is given by

$$u_i^t = u_{o_i}\left(1 + \overline{\lambda}\,\xi_i^t\right) \qquad i = 1,\ldots,\hat{n}_d \qquad t = 1,\ldots,T \tag{2.26}$$

Where $\bar{\lambda}$ is a fraction of the computed deformation u_o which controls the magnitude of error. Proportional errors are representative of actual measurement errors when all instruments are set to optimal sensitivity. True experimental errors lie somewhere between the bounds of absolute and proportional errors. The amplitude of absolute error λ, and the fraction parameter of proportional error $\bar{\lambda}$ are referred to as the magnitude of noise in the rest of this study.

2.4.3.2 Statistical indices

In a noisy environment, the parameters being estimated behave as random variables. To study estimation algorithms and to find trends in the behavior of these estimators, statistical indices can be used to characterize the results. A few appropriate statistical indices are introduced for use in probing the behavior of the algorithms by simulation (Banan and Hjelmstad, 1993).

The mean average $\bar{x}$ of the estimation sample $\{x^t, t = 1,..., T\}$ approximates the expected value of the estimated parameters E[x] and is computed as

$$\bar{x} = \frac{1}{T}\sum_{t=1}^{T} x^t \tag{2.27}$$

Where x^t is the vector of estimates for the tth trial. We refer to $\bar{x}$ as the vector of estimated parameters for a complete ensemble of trials. The mean average indicates the centroid of the distribution of the estimates in the space of parameters for a given experiment.

The quadratic bias $\|E[x]-\hat{x}\|^2$ is a measure of the distance between the centroid (expected value) of the estimates and the actual parameters $\hat{x}$ (which are known since simulation is being done). The average root quadratic bias (RQB) is defined as

$$RQB=\frac{\|\bar{x}-\hat{x}\|}{n_p\|\hat{x}\|} \tag{2.28}$$

Where n_p is the number of parameters and $\|\bar{x}-\hat{x}\|$ is the root quadratic bias of the sample. The RQB is normalized with respect to the norm of actual parameters.

The average standard deviation (SD) of the estimates, normalized with respect to $\|\hat{x}\|$ is given by

$$SD=\frac{\left[\frac{1}{T-1}\sum_{t=1}^{T}\sum_{i=1}^{n_p}\left(x_i^t-\bar{x}_i\right)^2\right]^{\frac{1}{2}}}{n_p\|\hat{x}\|} \tag{2.29}$$

The SD indicates the standard deviation, an approximation of the square root of the variance $E[(x - E[x])^2]$ of the estimates, and is a measure of scatter of the distribution of the estimates around the expected value. Bias and standard deviation are quantitative measures of accuracy and precision of an estimator, respectively. The smaller bias and standard deviation are, the more accurate and precise an estimator is.

When the set of parameters contains different types of quantities, such as axial, shear, or flexural stiffnesses, the statistical indices are computed by weighted averaging. For example, if there are three different types of parameters, then the average root quadratic bias is calculated as follows

$$RQB = \frac{1}{n_p^2} \sum_{i=1}^{3} n_{p_i}^2 RQB_i \tag{2.30}$$

Where n_{p_i} is the number of ith type parameters and RQB_i is computed based on Eqn. (2.28) whose variables are calculated for the set of estimates and actual values for the ith type of parameters.

3. FINITE ELEMENT MODELS FOR THE TCF BANK STADIUM AND THE THREE SPAN BEAM (TSB)

3.1 Finite element model for TCF Bank Stadium

TCF Bank Stadium is a relatively new stadium constructed in 2009 that has a current capacity of 50,805 people with the possibility to increase it to 80,000 in the near future. Figure 6 provides a plan view of the stadium as it was in 2013.

Figure 6. Plan View of the TCF Bank Stadium 2013

The girders and the risers that make the upper and lower decks in addition to some columns in the lower deck were constructed using a precast, post-tensioned concrete structural system. Furthermore, structural steel was used in elements like

columns in the upper level, the flooring system in areas such as the main concourse and elements to provide lateral bracing in specific locations of the stadium. For this study, special consideration will be given to the east end of the stadium where the student section is located due to the fact that young people would be likely more involved in periodic or rhythmic motions such as jumping or dancing.

The east lower deck is broken up into 8 typical sections. Each section is composed of precast seating single risers (stem equal to zero) resting on precast, post-tensioned, prismatic, concrete girders (rakers) or in some cases precast wall panels of 6" in thickness. There are also precast columns that support the main concrete girders. Figure 7 shows an elevation view of the lower deck in the east end of the stadium.

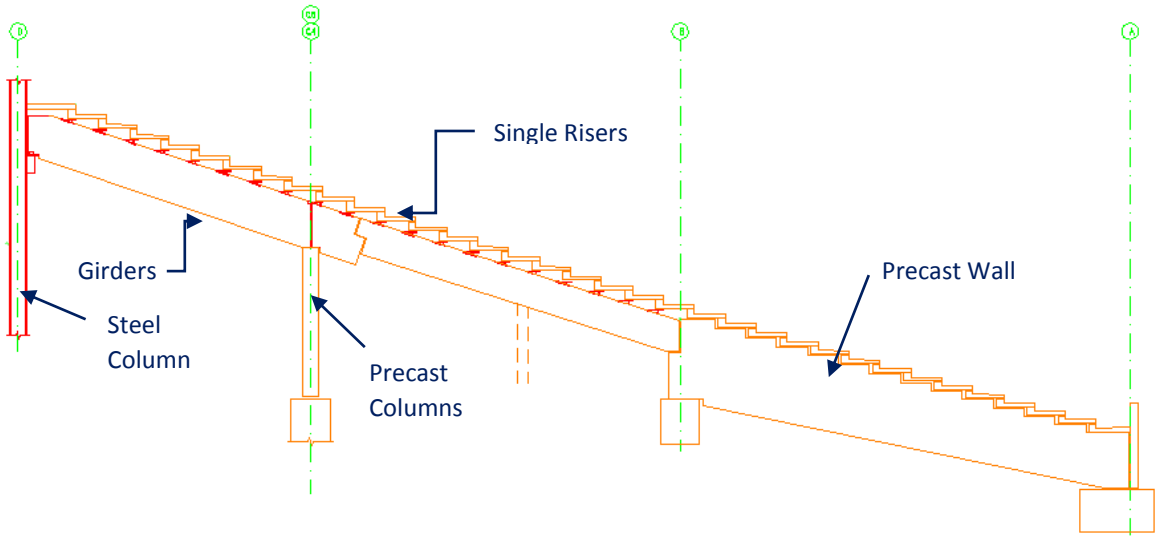

Figure 7. Elevation view of the lower deck in east end of stadium

Likewise the east upper deck is broken up into 10 typical sections. Each section is composed of precast seating single risers (with stem different than zero) resting on precast, post-tensioned, prismatic, concrete girders. Steel columns support the main

girders in the upper deck. Figure 8 shows an elevation view of the upper deck in the east end of the stadium.

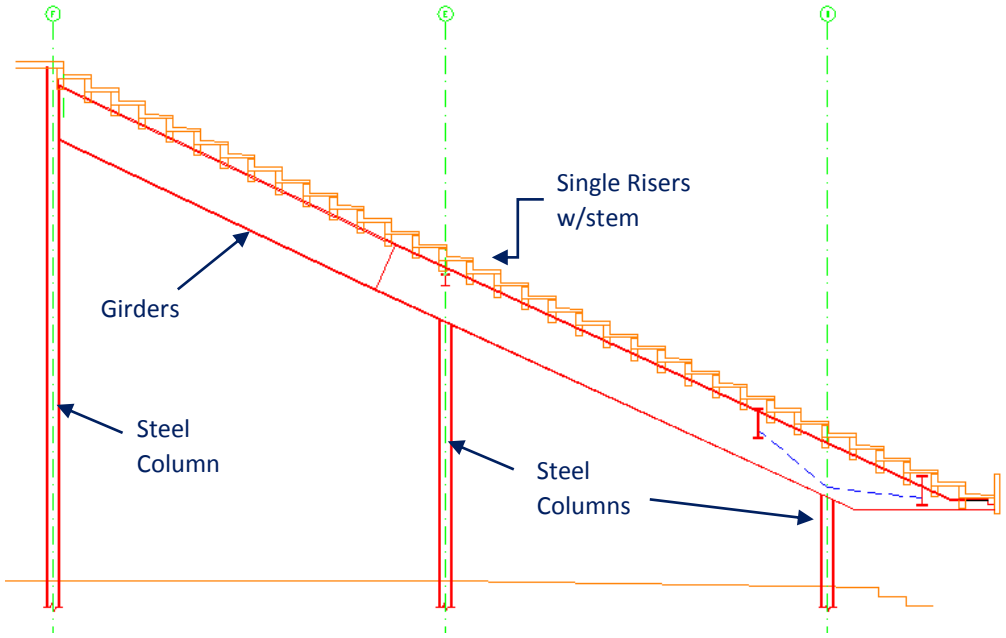

Figure 8. Elevation view of the upper deck in east end of stadium

The dimensions of the single risers with and without stem are presented in figure 9.

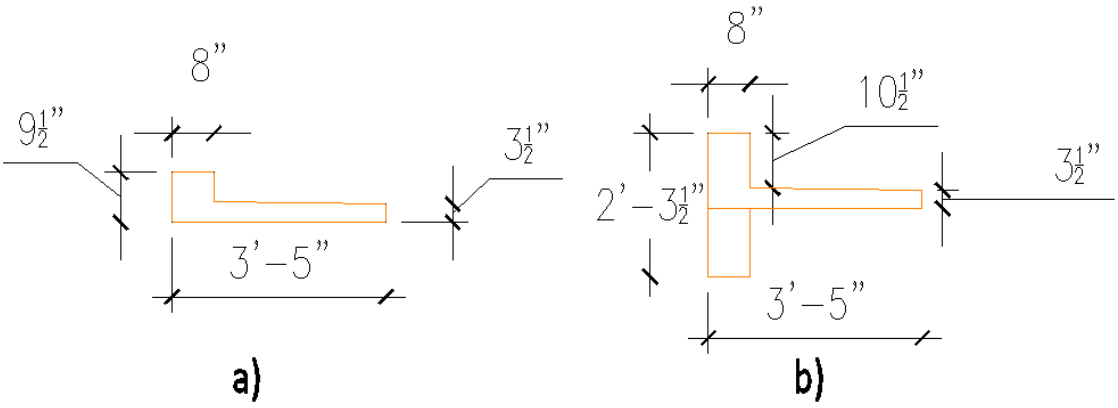

Figure 9. a) Single riser without stem and b) Single riser with stem

The finite element model of the east end of the stadium is created using the structural analysis program Staad.Pro V8i. To create the model, construction drawings of the east lower and upper decks of the TCF Bank Stadium were obtained from the consulting firm Magnusson Klemencic Associates.

All structural precast concrete elements (columns, risers, girders, walls) should have a compressive strength of 5,000 psi as per construction drawings and reinforced with ASTM A615, grade 60 steel in accordance with ACI-318 2005. The unit weight of concrete is considered as 150 pounds per cubic foot. In addition, precast units contain prestress as required by the contractor's design, which makes difficult the task of knowing exactly the reinforcement an element has.

All steel conforms to the following ($E = 29x10^6$ psi):

- W Shapes — ASTM A992, Fy = 50 ksi
  ASTM A913, Fy = 50 ksi
- Square or rectangular structural tube (HSS) — ASTM A500, Grade B, Fy = 46 ksi
- Round structural tube (HSS) — ASTM A500, Grade B, Fy = 42 ksi

The precast girders used to construct the stadium are prismatic members, which made the modeling process easy to carry out with the only exception of the girders located in the cantilever upper deck section. In that case the girder was broken up into smaller elements, each with different cross sectional properties obtained through linear interpolation given the dimensions of the element as per the elevation view of the upper deck as in figure 8, and using the average cross sectional area and moment of inertia of that smaller element. The modulus of elasticity associated with the concrete is based on the concrete specified design strength of 5,000 psi and calculated using the ACI 318-05 recommended equation:

$$E_c = (w_c)^{1.5}(33)\left(\sqrt{f'c}\right) = (150)^{1.5}(33)\left(\sqrt{5{,}000}\right) = 4{,}286.825 ksi$$

The girder in the lower deck is modeled with hinges at the nodes where there is a column supporting it due to the fact that the girder is not a continuous element. However, the girders in the upper deck are modeled as a continuous element as shown in the construction drawings. The risers are modeled with hinges at both ends where they are supported by the girders, in other words, as simply supported beams. The precast and steel columns are modeled in such a way that the top end of the elements is released from bending moments, due to the fact that the connection between precast girders and columns is not fixed, actually simply supported, as opposed to cast in place elements where the degree of fixity is higher.

The fact that only the east end of the stadium is modeled brings one difficulty as to what would be the appropriate boundary conditions where the "cut" was made. The approach that was used to model this is the following:

- The complete beam (riser) that is truncated is analyzed in order to determine the deflection in the vertical direction due to concentrated vertical loads resembling the crowd loading using the method of virtual work or the "dummy load" *at the location of the cut*.
- After computing the deflection in terms of the Young's modulus and the moment of inertia, we compute the equivalent stiffness of the beam using the relation ku = f, where k is the stiffness, u is the vertical displacement and f is the set of concentrated forces acting on the beam. Note that the concentrated forces are assumed to be equal.
- Having computed the stiffness, we put linear springs at the locations where the cut was made in the global directions (Y, X and Z). One

assumption made here is that the local x and z axes of the risers do not vary too much from the X and Z global directions.

Figure 10 shows the beam used to determine the spring constants for the risers in the upper deck of the east end of the stadium using the procedure discussed previously. The red dot shown in the figure represents the location where the displacement was calculated.

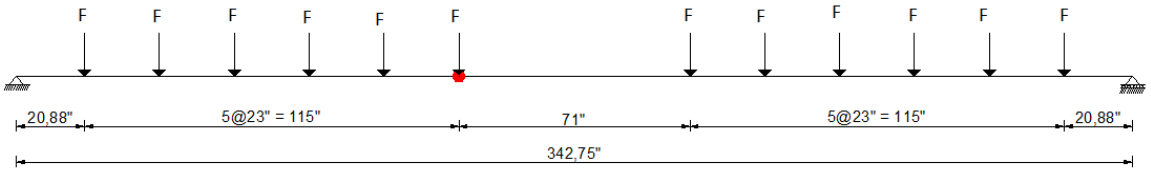

Figure 10. Beam used to compute spring constant in the upper deck of stadium

Similarly, figure 11 shows the beam used to determine the spring constants for the risers in the lower deck of the east end of the stadium. Again the red dot indicates the location where the displacement was computed.

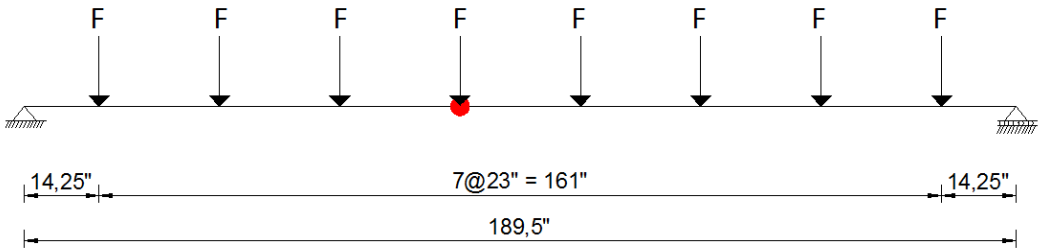

Figure 11. Beam used to compute spring constant in the lower deck of stadium

The spring constants obtained were k = 9,907.45 lb/in for the risers in the upper deck of the stadium and k = 5,643.21 lb/in for the risers in the lower deck. For ease of analysis, these spring constants will be applied in the three global directions. Figure 12 shows how the program Staad.Pro identifies linear springs.

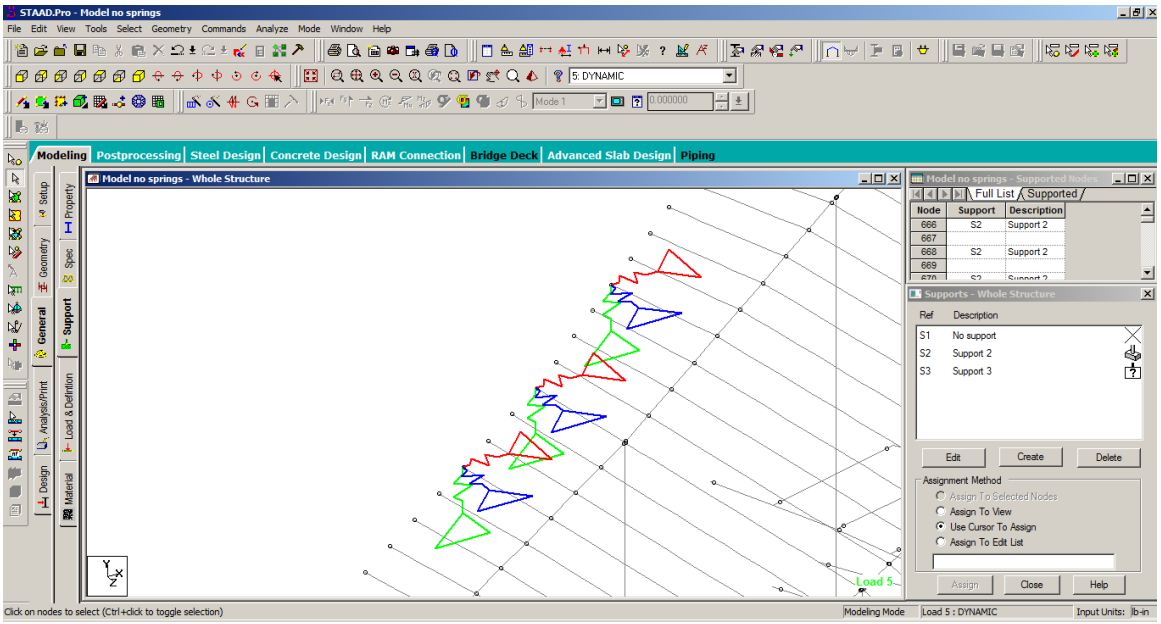

Figure 12. Identification of linear springs in Staad.Pro (X = red, Y = green, Z = blue)

Figure 13 shows the complete model of the east end of the TCF Bank Stadium that captures the presence of the linear springs as computed previously and the member releases (hinges) wherever marked on the construction drawings.

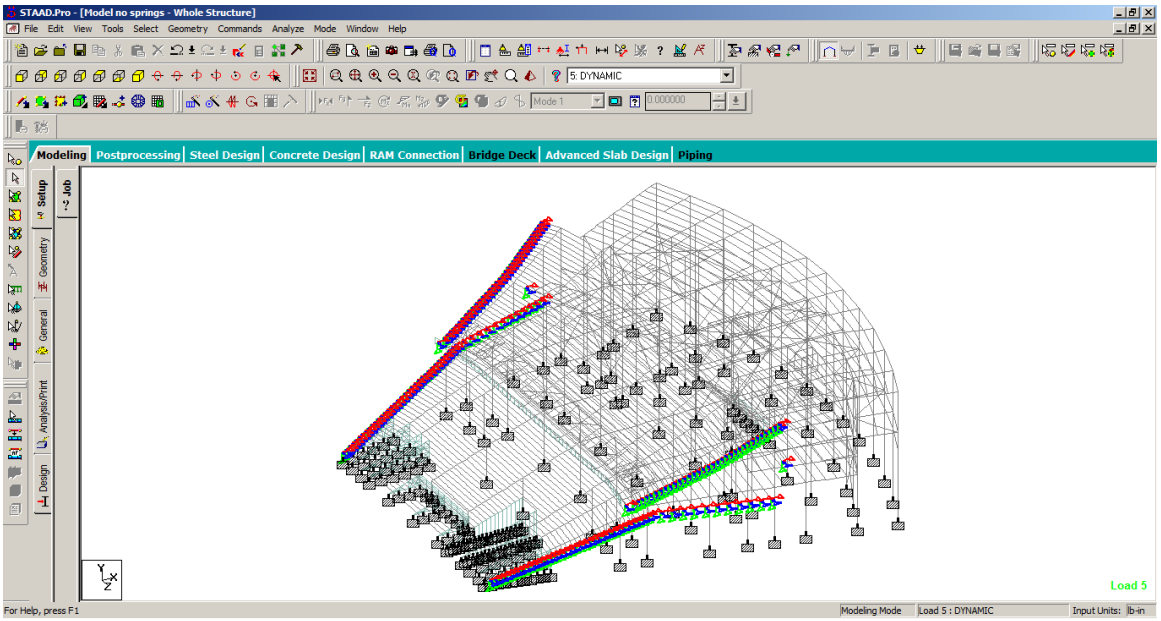

Figure 13. Complete model of the east end of the stadium in Staad.Pro

3.2 Finite element model for TSB

In order to gain more insight on the problem at hand and also to check the solution given by the Matlab program created to perform a modal analysis against the solution given by Staad.Pro, a three span beam model with the element properties of a riser in the upper deck will be used. The reason why a three span beam model is selected is mainly because that is the area where the length of the beams is greater, close to 43 feet, thus it is expected a higher response, whether it is in terms of displacements, accelerations or stresses.

Figure 14 presents the three span beam that will be used. It is interesting to note that the supports are modeled as linear springs since the risers are supported by the girders and also that there are hinges at both ends of the beams since the connection does not provide a total fixity condition, simulating a simply supported beam.

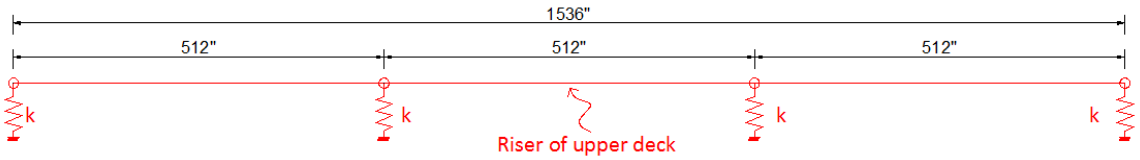

Figure 14. Three span beam model

In order to know the stiffness of those linear springs a procedure similar to that explained in the previous section is performed on the girders. The only difference being that the average stiffness is taken since there are several risers that are supported by the girder. Figure 15 shows the model of the girder used to compute the stiffness used in the TSB.

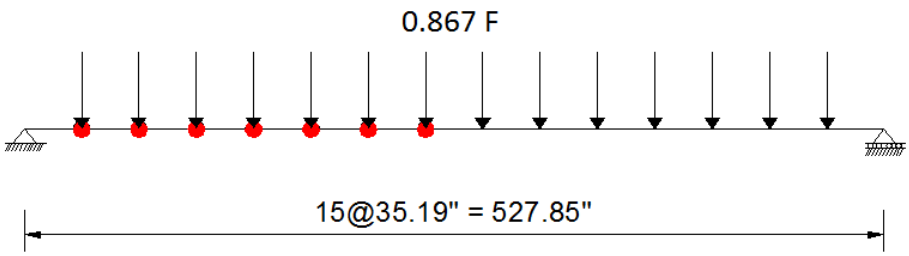

Figure 15. Girder model to compute the stiffness of the linear springs in the TSB

All of the concentrated loads are equal to 0.867F due to the fact that the girder makes an angle of 29.885° with the horizontal. Using the method of virtual work the displacements are computed at the locations where the red dots are present. Knowing the 7 displacements in terms of the force F, elastic modulus E and moment of inertia I, we get 7 stiffnesses which later the average is computed and that is the value used for the TSB model shown in figure 14. The stiffness thus obtained is equal to 71,621.71 lb/in.

4. DYNAMIC ANALYSIS OF THE TCF BANK STADIUM AND TSB USING HUMAN-STRUCTURE INTERACTION CONCEPTS

4.1 Results for the TSB from static analysis

Just for the sake of comparison, a static analysis was performed on the TSB with the loading of 100 lb/ft^2 of live load specified in the ASCE 7-10. The load factors were taken as 1.2 for the dead load and 1.6 for the live load, as per the current codes (ASCE 7-10, ACI 318-10). In addition, load factors of 1.4 and 1.7 for the dead and live loads respectively were used as per the older versions of the previously mentioned codes or standards. Table 5 presents the results of the static analysis in terms of the maximum displacement, maximum shear force and maximum bending moment in one of the risers of the upper level.

Table 5. Results from static analysis in the TSB

Static Analysis	Max. Displacement (in)		Max. Shear Force (lb)	Max. Bending Moment (kips in)
Static (1.2 DL, 1.6 LL)	1.58	-	17,672.92	2,262.13
Older load factors				
Static (1.4 DL, 1.7 LL)	1.76	-	19,718.99	2,524.03

4.2 Results for the TSB from dynamic analysis

4.2.1 All people in the TSB active

Table 6 presents the results of the dynamic analysis of the TSB for the case of having 60 people active (jumping/dancing) for different excitation frequencies.

Table 6. Results from dynamic analysis in the TSB for different excitation frequencies

All active (60 people)	Max. Displacement (in)	Max. Acceleration (m/s^2)	Max. Shear Force (lb)	Max. Bending Moment (kips in)
1.8Hz	1.01	1.74	10,354.84	1,579.60
1.97Hz	1.55	3.26	15,881.61	2,421.46
2.13Hz	1.66	4.19	17,135.09	2,622.28
2.3Hz	0.90	2.31	9,190.56	1,402.71

One thing worth mentioning is that the first natural frequency of the TSB is 4.327 Hz. By looking at table 6 we can see that the 2.13 Hz excitation frequency produces the highest response, because the second harmonics (4.26 Hz) of this frequency is very close to the natural frequency of the TSB, therefore the possibility of resonance is increased for this particular case. Furthermore, we can see that the acceleration of 4.19 m/s^2 is more than the limiting value given by Kasperski M. (1996) in table 4 of 35% of g (3.43 m/s^2). In addition, this response is greater than the one predicted by the static analysis from table 5, using the load factors of 1.2 for dead load and 1.6 for live load, which means that a dynamic analysis must be performed in order to study the effects of people jumping/dancing at different frequencies.

4.2.2 Maximum response in the TSB for different locations of active/passive people

Several cases were studied in order to determine how much of active and passive people would be required so that the response would be a maximum, whether it is in terms of displacement, acceleration, shear force and bending moment. Additionally, the location of the active and passive people was varied along the length of the TSB to see if this affects the response as well. The results are shown in table 7.

Table 7. Results from dynamic analysis in the TSB for different excitation frequencies, different number of active and passive people, and different location of the people

With some passive people (standing)	Max. Displacement (in)	Max. Acceleration (m/s^2)	Max. Shear Force (lb)	Max. Bending Moment (kips in)
1.80 Hz	1.01	1.74	10,354.84	1,579.60
1.97 Hz	1.55	3.26	15,881.61	2,421.46
2.13 Hz	**1.67**	**4.20**	**18,313.2**	**2,739.78**
2.30 Hz	**1.15**	**3.29**	**13,794.3**	**2,133.30**

For the cases of having an excitation frequency of 1.8 and 1.97 Hz, the maximum response was the same as the case of having all active people (table 6). However, for the cases of 2.13 and 2.30 Hz in excitation frequency, the maximum response was obtained by reducing the amount of active people and by changing the location of the passive people as can be seen in figures 16 and 17.

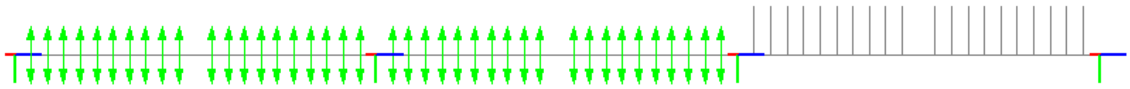

Figure 16. Active people and passive people configuration for an excitation frequency of 2.13 Hz that gives maximum response

Figure 17. Active people and passive people configuration for an excitation frequency of 2.30 Hz that gives maximum response

It is interesting to note as well that the natural frequencies for the TSB shown in figures 16 and 17 got reduced, due to the presence of passive people. The frequencies were 4.035 Hz and 3.987 Hz for the configurations in figures 16 and 17, respectively. Even though the second harmonic of the two excitation frequencies is not exactly equal

to the natural frequency of the TSB, it was observed that the frequencies of the higher modes (especially 2 and 3) were very close to the excitation frequencies of the active people.

4.2.3 Response in the TSB for different locations with a ratio active/passive people equal to one

The case of having a ratio of active to passive people equal to one was studied, in other words, 30 people active and 30 people passive in the TSB. The results were carried out for the four excitation frequencies.

Figures 18 and 19 show the configurations of active and passive people that led to minimum and maximum responses, respectively for an excitation frequency of 1.80 Hz. In addition, table 8 shows the results for this excitation frequency.

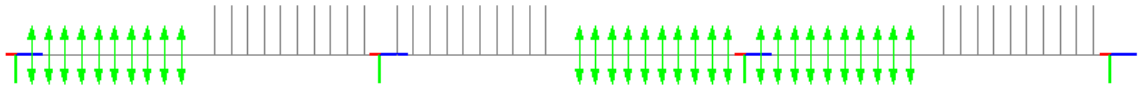

Figure 18. Configuration of active/passive people for minimum response (Excitation frequency of 1.8 Hz)

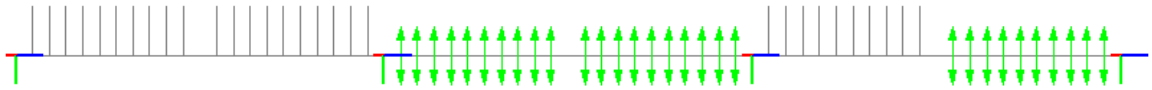

Figure 19. Configuration of active/passive people for maximum response (Excitation frequency of 1.8 Hz)

Table 8. Minimum and maximum response from dynamic analysis in the TSB for an active to passive ratio of one and excitation frequency of 1.8 Hz

	Max. Vertical Displacement (in)	Max. Acceleration (m/s^2)	Max. Shear Force (lb)	Max. Bending moment (kip in)
Min	0.627	1.07	6,517.30	977.59
Max	0.687	1.3155	7,326.08	1,114.58

For this case, the difference in responses is not that much different, possibly due to the fact that the natural frequencies of the beams in figures 18 and 19 are 4.055 and 4.027 Hz, respectively which are roughly equal, thus similar responses are present.

Figures 20 and 21 show the configurations of active and passive people that led to minimum and maximum responses, respectively for an excitation frequency of 1.97 Hz, as well as table 9 where the responses are presented.

Figure 20. Configuration of active/passive people for minimum response (Excitation frequency of 1.97 Hz)

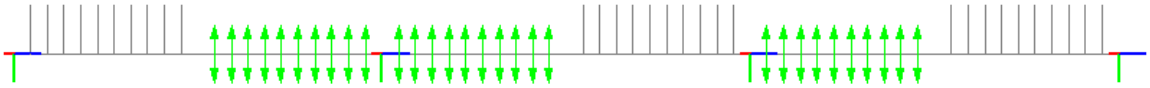

Figure 21. Configuration of active/passive people for maximum response (Excitation frequency of 1.97 Hz)

Table 9. Minimum and maximum response from dynamic analysis in the TSB for an active to passive ratio of one and excitation frequency of 1.97 Hz

	Max. Vertical Displacement (in)	**Max. Acceleration (m/s^2)**	**Max. Shear Force (lb)**	**Max. Bending moment (kip in)**
Min	0.739	1.485	8,530.80	1,329.60
Max	1.06	2.31	11,671.10	1,685.40

In this case the difference is more pronounced since the natural frequency of the TSB in figure 21 is 3.947 Hz, which is almost the same as the second harmonic of the excitation frequency of 1.97 Hz, whereas the frequency of the TSB in figure 20 is 4.072 Hz.

Furthermore, figures 22 and 23 show the configurations of active and passive people that led to minimum and maximum responses, respectively for an excitation frequency of 2.13 Hz, in addition to table 10 where the responses are presented.

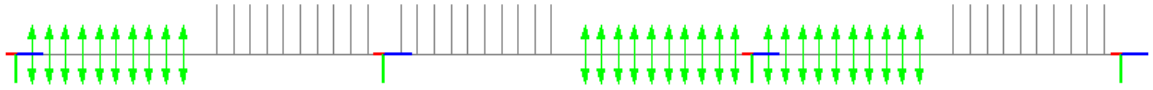

Figure 22. Configuration of active/passive people for minimum response (Excitation frequency of 2.13 Hz)

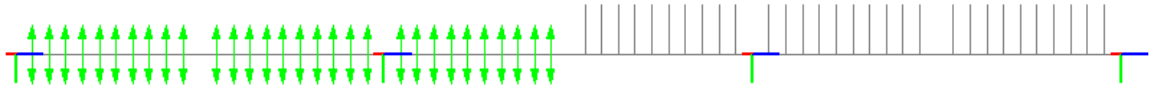

Figure 23. Configuration of active/passive people for maximum response (Excitation frequency of 2.13 Hz)

Table 10. Minimum and maximum response from dynamic analysis in the TSB for an active to passive ratio of one and excitation frequency of 2.13 Hz

	Max. Vertical Displacement (in)	**Max. Acceleration (m/s^2)**	**Max. Shear Force (lb)**	**Max. Bending moment (kip in)**
Min	0.482	1.1115	5,539.02	770.14
Max	1.01	2.325	11,376.50	1,748.70

Similarly for this case, the second harmonic of the excitation frequency is closer to the natural frequency of the TSB shown in figure 23 of 4.055 Hz than it is to the natural frequency of the TSB in figure 22 of 3.975 Hz. The response in this case is bigger by a factor of 2 or so, for all of the responses studied.

Lastly, figures 24 and 25 show the configurations of active and passive people that led to minimum and maximum responses, respectively for an excitation frequency of 2.30 Hz, and table 11 that presents the computed responses.

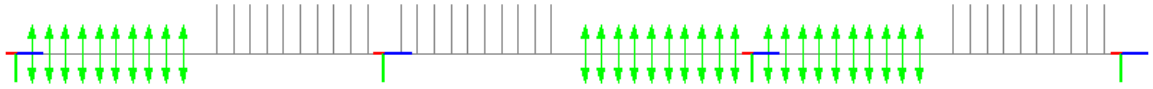

Figure 24. Configuration of active/passive people for minimum response (Excitation frequency of 2.30 Hz)

Figure 25. Configuration of active/passive people for maximum response (Excitation frequency of 2.30 Hz)

Table 11. Minimum and maximum response from dynamic analysis in the TSB for an active to passive ratio of one and excitation frequency of 2.30 Hz

	Max. Vertical Displacement (in)	**Max. Acceleration (m/s^2)**	**Max. Shear Force (lb)**	**Max. Bending moment (kip in)**
Min	0.328	0.7395	3,601.28	542.32
Max	1.11	3.21	13,106.99	2,035.85

The difference in this case is more pronounced, about a factor of 3.5 to 4 for all of the responses. Again, it seems that the second harmonic of the excitation frequency (4.60 Hz) adds significant more energy into the system of figure 25, where the natural frequency is 4.124 Hz. The low values for the minimum case are an indicative that the configuration of figure 24 adds significant amount of damping into the system.

4.3 Results for the TCF Bank Stadium from static analysis

A static analysis was performed on the section of the stadium in order to have some numerical values so we can compare them with the results obtained from the dynamic analyses. Table 12 shows the maximum response in three different elements, specifically riser, girder and cantilever.

Table 12. Maximum response in three different structural elements of the stadium from static analysis

	Vertical Displacement (in)	Shear Force (lb)	Bending moment (Kip in)
Cantilever	1.65	58,625.40	8,326.90
Riser	1.58	17,672.92	2,262.13
Girder	0.698	132,594.20	19,140.80

4.4 Results for the TCF Bank Stadium from dynamic analysis

4.4.1 All people active

Dynamic analyses were performed in the section of the stadium with four different excitation frequencies, 1.8, 1.97, 2.13 and 2.30 Hz, for the case of having all of the people active. Tables 13, 14 and 15 show the results for each of the structural elements and for each of the excitation frequencies.

Table 13. Maximum response in risers from dynamic analysis

	Vertical Displacement (in)	Shear Force (lb)	Bending moment (Kip in)	Acceleration (m/s^2)
1.8 Hz	1.95	16,887.15	2,490.35	3.34
1.97 Hz	2.22	20,054.80	2,984.70	4.74
2.13 Hz	1.51	13,632.10	2,063.90	3.55
2.30 Hz	1.04	10,481.10	1,603.20	2.58

It can be seen from the table that the excitation frequency of 1.97 Hz gives the highest response in the risers. The level of acceleration obtained is close to 0.5g which according to Kasperski M. (1996) would be considered as an acceleration that is causing panic in the audience. It can be seen that the response from the static analysis is greater than the one obtained for the excitation frequencies of 2.13 and 2.30 Hz. The possible reason for the difference in results from the TSB and the complete stadium is that

averages of spring constants were taken for the TSB, whereas for the stadium, the actual girder is supporting the risers.

Table 14. Maximum response in girders from dynamic analysis

	Vertical Displacement (in)	Shear Force (lb)	Bending moment (Kip in)	Acceleration (m/s^2)
1.8 Hz	0.858	270,935.10	44,578.30	2.67
1.97 Hz	0.802	158,507.90	27,944.50	1.8
2.13 Hz	0.531	109,486.80	16,758.60	1.11
2.30 Hz	0.432	96,812.40	14,626.30	0.77

For the case of the girders, the excitation frequency of 1.8 Hz gives the highest response, but in this case the levels of acceleration are below the limiting value defined in table 4, however the acceleration of 2.67 m/s^2 is still in the range of "unacceptable". Comparing these values against the ones obtained from static analysis, it can be observed that again the excitation frequencies of 1.8 and 1.97 Hz gave higher values for the quantities measured as was the case for the risers.

Table 15. Maximum response in cantilever from dynamic analysis

	Vertical Displacement (in)	Shear Force (lb)	Bending moment (Kip in)	Acceleration (m/s^2)
1.80 Hz	1.52	45,837.70	6,839.16	1.51
1.97 Hz	1.42	42,296.60	6,647.60	1.49
2.13 Hz	1.81	61,481.04	8,474.48	1.695
2.30 Hz	2.69	81,393.80	11,347.60	2.59

For the cantilever beams the excitation frequencies of 2.13 and 2.30 Hz gave responses higher than those obtained from static analysis. One of the reasons this is so for this type of beam is that the first mode shape of a riser or a girder which involves vertical motion might not be the same as for the cantilever beam, thus the excitation frequencies of 2.13 and 2.30 Hz might have excited a different mode shape for the

cantilever beams, as opposed for the risers and girders, where the excitation frequencies of 1.8 and 1.97 Hz gave the highest response.

4.4.2 Response in the TCF Bank Stadium as per load cases determined from the TSB results

Tables 16 and 17 show the results from dynamic analyses with an excitation frequency of 1.8 Hz for the cases of having an active to passive ratio of one as per figures 18 and 19, respectively.

Table 16. Response in stadium with loading case as per figure 18, with 1.8 Hz excitation frequency

	Displacement (in)	**Acceleration (m/s^2)**	**Shear force (lb)**	**Moment (Kip in)**
Riser	1.13	1.98	10,393.50	837.65
Girder	0.54	0.88	153,456.70	26,788.50
Cantilever	0.89	0.77	34,387.20	4,025.75

Table 17. Response in stadium with loading case as per figure 19, with 1.8 Hz excitation frequency

	Displacement (in)	**Acceleration (m/s^2)**	**Shear force (lb)**	**Moment (Kip in)**
Riser	1.39	2.37	14,675.50	1,231.70
Girder	0.64	1.27	197,238.70	31,797.80
Cantilever	1.01	0.86	40,387.60	4,873.20

From table 17 it can be observed that the responses in the three structural elements is between 65% and 75% of the response with all people active. Furthermore, in terms of serviceability and in particular the level of acceleration, the maximum observed in table 17 of 2.37 m/s^2 or 0.24g is below the limiting value of 0.35g, but is between the levels of disturbing and unacceptable, thus a dynamic analysis like the one performed here would be appropriate for this excitation frequency. The absolute maximum

response for 1.8 Hz excitation frequency is still observed in tables 13, 14 and 15 for the risers, girders and cantilevers, respectively.

Additionally, tables 18 and 19 show the results from dynamic analyses with an excitation frequency of 1.97 Hz for the cases of having an active to passive ratio of one as per figures 20 and 21, respectively.

The response for this case of 1.97 Hz excitation frequency produces higher values of the measured parameters than those obtained in the previous case of 1.8 Hz. Compared to the values obtained from the case of having all active people, with a ratio of active/passive people of one, the response can be decreased from percentages of 30% to 35%. For example, having all people active produces 4.74 m/s^2 of acceleration in the riser which is clearly above the limit proposed by Kasperski, M. (1996), whereas the result in table 18 shows an acceleration of only 2.41 m/s^2. Similar comparisons can be performed, but the point is that the location of the passive people can be varied in order to decrease the response in the stadium in any given moment.

Table 18. Response in stadium with loading case as per figure 20, with 1.97 Hz excitation frequency

	Displacement (in)	**Acceleration (m/s^2)**	**Shear force (lb)**	**Moment (Kip in)**
Riser	1.53	2.41	14,873.50	1,798.50
Girder	0.51	0.81	102,729.40	13,275.24
Cantilever	0.84	0.71	28,830.11	4,111.31

Table 19. Response in stadium with loading case as per figure 21, with 1.97 Hz excitation frequency

	Displacement (in)	**Acceleration (m/s^2)**	**Shear force (lb)**	**Moment (Kip in)**
Riser	1.91	3.01	18,713.20	2,273.10
Girder	0.68	1.13	139,613.20	20,393.20
Cantilever	1.20	0.97	39,757.30	5,873.31

Tables 20 and 21 show the results from dynamic analyses with an excitation frequency of 2.13 Hz for the cases of having an active to passive ratio of one as per figures 22 and 23, respectively. Furthermore, table 22 shows the results from the loading case that gave the highest response with 2.13 Hz in the TSB, as per figure 16.

Table 20. Response in stadium with loading case as per figure 22, with 2.13 Hz excitation frequency

	Displacement (in)	**Acceleration (m/s^2)**	**Shear force (lb)**	**Moment (Kip in)**
Riser	0.64	1.41	6,713.70	1,104.50
Girder	0.24	0.52	54,587.30	7,397.70
Cantilever	0.77	0.72	25,726.80	3,706.80

Table 21. Response in stadium with loading case as per figure 23, with 2.13 Hz excitation frequency

	Displacement (in)	**Acceleration (m/s^2)**	**Shear force (lb)**	**Moment (Kip in)**
Riser	1.13	2.48	11,778.50	1,937.80
Girder	0.39	0.88	95,767.30	12,978.50
Cantilever	1.43	1.33	43,729.80	6,327.80

Table 22. Response in stadium with loading case as per figure 16, with 2.13 Hz excitation frequency

	Displacement (in)	**Acceleration (m/s^2)**	**Shear force (lb)**	**Moment (Kip in)**
Riser	1.61	4.13	17,813.90	2,639.80
Girder	0.62	1.15	115,917.50	17,123.90
Cantilever	1.79	1.63	57,879.50	8,018.90

From tables 20 and 21, it can be seen that for an equal number of active and passive people, the maximum response obtained is somewhere between 70% and 80% of the response obtained from the case of having all people active. In terms of how the location of the passive people reduces the acceleration of the risers and therefore all the

other structural elements, it can be noted that from an acceleration of 3.55 m/s² in the riser having 60 active people gets reduced to 1.41 m/s², or a reduction of 60%.

Table 22 shows that actually having all people active does not yield the maximum response in the structural elements of the stadium. The loading case shown in figure 16 presents to the structure higher response. Acceleration level of 4.13 m/s² can be seen, which is in the range of causing panic, the maximum displacement in the riser increased about 6%, the maximum displacement in the girder increased 16% and interestingly enough, the displacement in the cantilever decreased by 1.1%. One of the reason for this behavior is that the cantilever portion of the stadium, and in general any stadium, tend to have mode shapes, and therefore natural frequencies, that are different than those obtained for the risers or girders. One other possible reason is that this excitation frequency may be exciting, perhaps with the second harmonic, local modes of the risers within the stadium.

Lastly, tables 23 and 24 show the results from dynamic analyses with an excitation frequency of 2.30 Hz for the cases of having an active to passive ratio of one as per figures 24 and 25, respectively. In addition, table 25 shows the results from the loading case that gave the highest response with 2.30 Hz in the TSB, as per figure 17.

Table 23. Response in stadium with loading case as per figure 24, with 2.30 Hz excitation frequency

	Displacement (in)	**Acceleration (m/s²)**	**Shear force (lb)**	**Moment (Kip in)**
Riser	0.41	0.81	3,971.30	631.20
Girder	0.17	0.55	87,373.50	11,724.30
Cantilever	1.27	1.13	59,327.30	7,987.60

Table 24. Response in stadium with loading case as per figure 25, with 2.30 Hz excitation frequency

	Displacement (in)	**Acceleration (m/s^2)**	**Shear force (lb)**	**Moment (Kip in)**
Riser	0.92	2.24	9,073.40	1,097.30
Girder	0.39	0.62	88,213.30	13,878.30
Cantilever	2.03	1.88	70,323.40	9,327.40

Table 25. Response in stadium with loading case as per figure 17, with 2.30 Hz excitation frequency

	Displacement (in)	**Acceleration (m/s^2)**	**Shear force (lb)**	**Moment (Kip in)**
Riser	1.22	2.69	12,327.40	1,693.20
Girder	0.47	0.83	99,798.20	15,203.40
Cantilever	2.04	1.88	70,424.30	9,359.70

Table 25 presents the response that is greater than the response from having all 60 people active. An acceleration of 2.69 m/s^2 can be seen in the riser, which is in the unacceptable range, the maximum displacement in the riser increased about 17%, the maximum displacement in the girder increased 8.8% and the displacement in the cantilever decreased by 24.16%. The reasons described earlier for the previous case apply here as well.

From tables 23 and 24, it can be seen that for an equal number of active and passive people, the maximum response obtained is somewhere between 75% and 93% of the response obtained from the case of having all people active. The acceleration of the risers and therefore all the other structural elements got reduced for the case of using the load case as depicted in figure 24, for instance, it can be noted that from an acceleration of 2.69 m/s^2 in the riser from table 25, it gets reduced to 0.813 m/s^2, or a reduction of 69%. A reduction of 33% in acceleration of the girder is present and a reduction of 56% for the cantilever beam.

4.5 Summary

After performing a dynamic analysis of the TSB, the results showed that for an excitation frequency of 2.13 Hz, the response of the TSB is greater than that produced by static analysis applying a load of 100 lb/ft^2 plus dead loads, using the load factors as per ASCE 7-10.

An analysis was carried out in order to determine the maximum response in the TSB for the four different excitation frequencies. The results showed that for the frequencies of 1.8 Hz and 1.97 Hz, the maximum response was obtained as a result of having 60 people active. The maximum response for an excitation frequency of 2.13 Hz was obtained for the configuration shown in figure 16, and the maximum response for an excitation frequency of 2.30 Hz was obtained for the configuration shown in figure 17.

Dynamic analysis showed that the response of some structural elements in the stadium (riser, cantilever, and girder) is sometimes greater than that obtained from static analysis.

After applying the different configurations of active/passive people for the specific cases of having an excitation frequency of 2.13 Hz and 2.30 Hz from figures 16 and 17 into the section of the stadium, it was observed in general an increase in the response, especially for the risers and girders. Interestingly, the response in the cantilever showed lower values when using these configurations, indicating that a local mode, of the risers, was probably excited more easily than the cantilever mode shape.

5. PARAMETER ESTIMATION RESULTS

5.1 Parameter estimation results for the TSB

In order to see whether or not the parameter estimation algorithms gave good results, analysis of the TSB was performed prior to the study of the section of the stadium for different combinations of number of measurements, number of degrees of freedom (dof's) measured and different values of absolute and proportional error. The absolute error used for this analysis was from 0.003 to 0.03 and the proportional error was between 1% and 10%.

5.1.1 Statistical indices

Figures 26 and 27 show the RQB and SD values for the TSB in the case of having measured 3 dof's and having performed 3 measurements, or in other words, having determined the first 3 mode shapes of the TSB for both the EEE and the OEE.

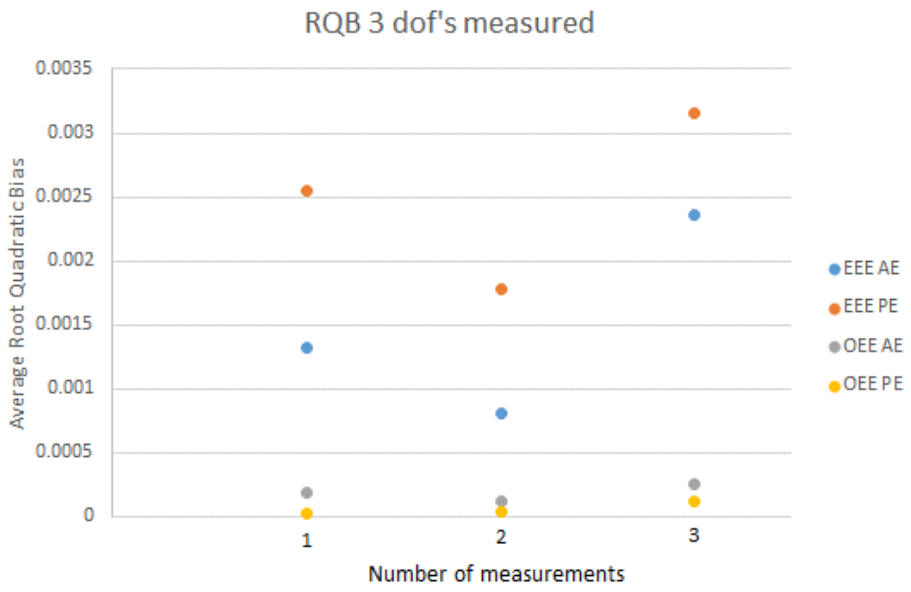

Figure 26. RQB values for TSB having 3 dof's measured and 1 to 3 measurements

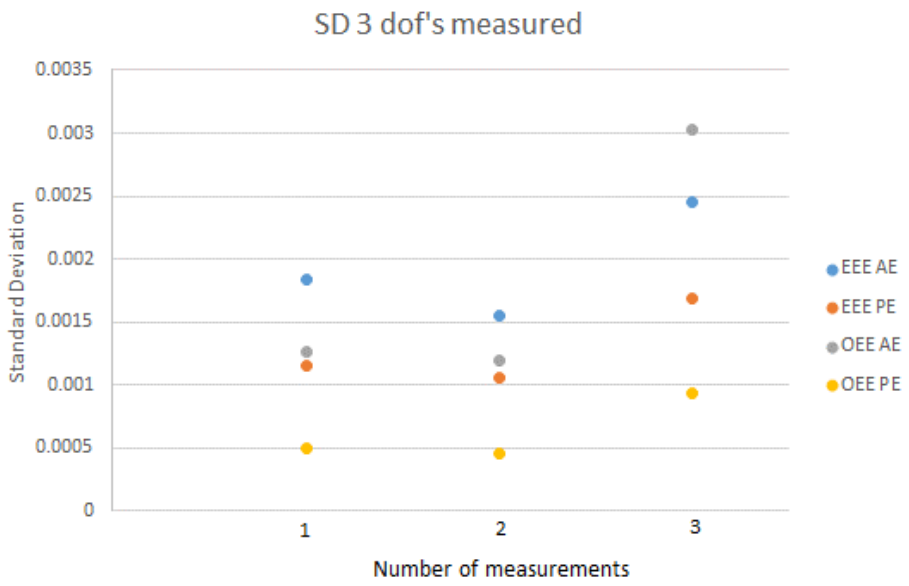

Figure 27. SD values for TSB having 3 dof's measured and 1 to 3 measurements

By looking at the figures it can be seen that the results get better as we move from 1 measurement to two measurements, however this behavior is not observed when going from 2 to three measurements, for both the estimators. The reason for this is that the third measurement does not add not enough new information for the system to obtain good values of the estimates, and in fact the new information produces worse results. One thing to notice as well is that the results are better all the time we have proportional error instead of having absolute error.

Figures 28 and 29 show the RQB and SD values for the TSB in the case of having measured 6 dof's and having performed 1 to 3 measurements for both the EEE and the OEE.

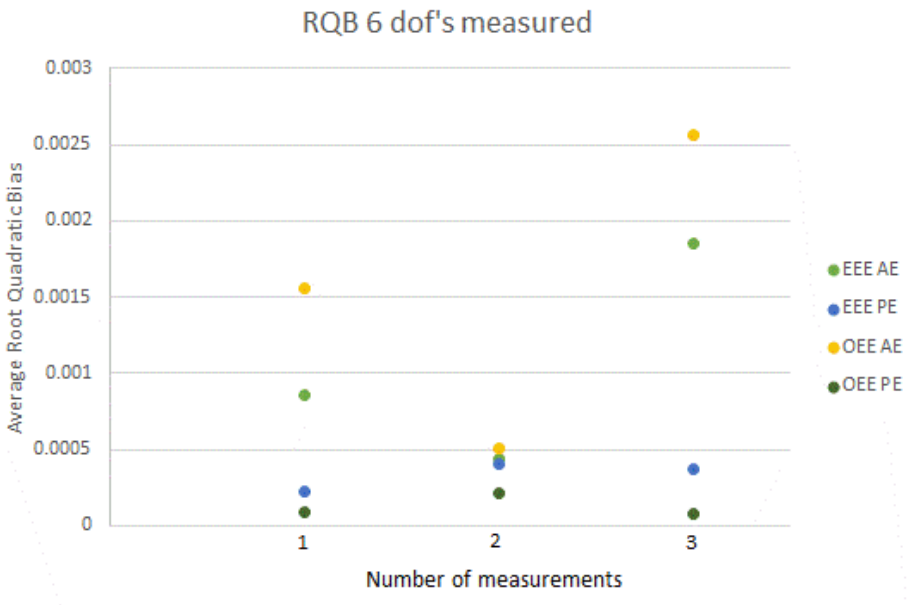

Figure 28. RQB values for TSB having 6 dof's measured and 1 to 3 measurements

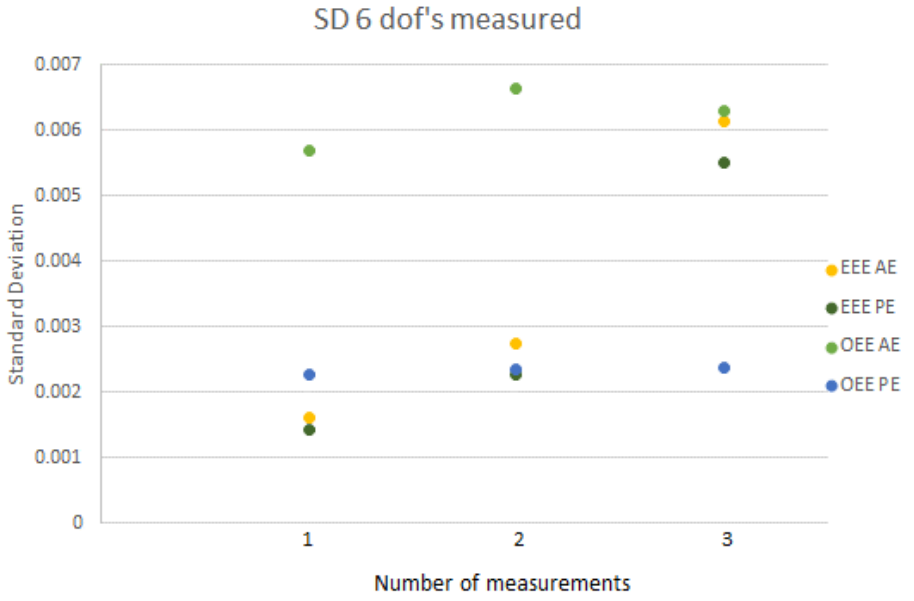

Figure 29. SD values for TSB having 6 dof's measured and 1 to 3 measurements

This case shows a similar behavior as the previous one, where the estimates become better as we move from 1 to 2 measurements but this time only for results that

have absolute error. Having 3 measurements produces the best results of RQB for the OEE with proportional error and the best results of SD are obtained from the EEE with proportional error with only 1 measurement.

Furthermore, figures 30 and 31 present the RQB and SD values for the TSB in the case of having measured 9 dof's and having performed 3 measurements for both the EEE and the OEE.

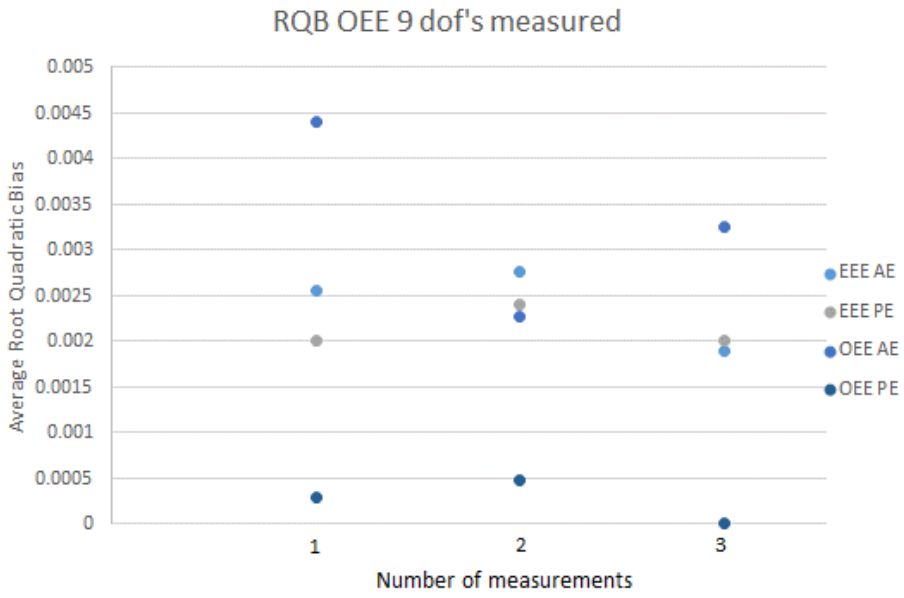

Figure 30. RQB values for TSB having 9 dof's measured and 1 to 3 measurements

From figure 30 it can be seen that for the OEE and proportional error the estimates are better when there are 3 measurements and the estimates are worse for the OEE and absolute error when there is only 1 measurement. For the EEE for both the absolute and proportional errors, the estimates are better when the measurements capture 3 mode shapes of the TSB. Similar outcome is present for the SD values shown in figure 31 with the only difference that the worst value of SD was obtained for the EEE and absolute error when there is only 1 measurement.

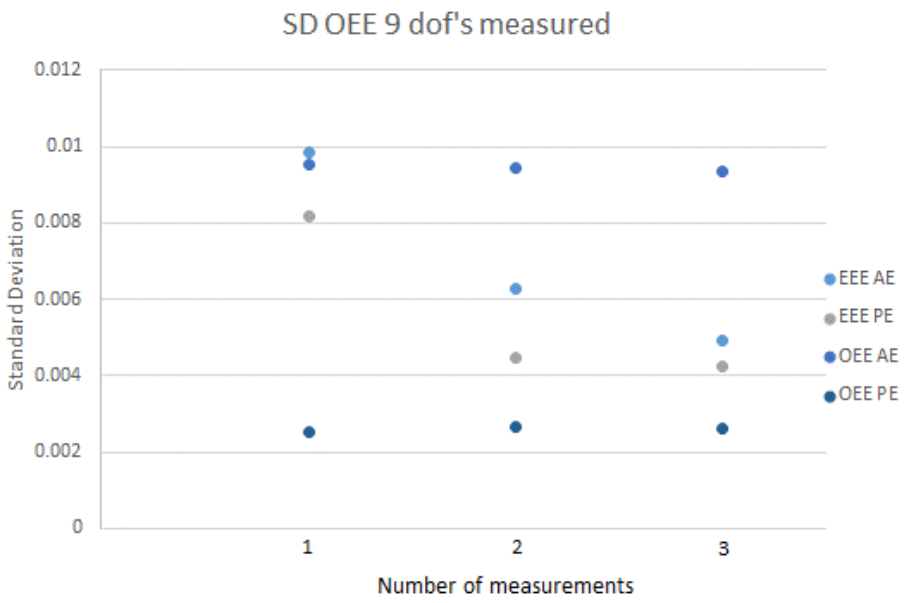

Figure 31. SD values for TSB having 9 dof's measured and 1 to 3 measurements

Figures 32 and 33 show the comparative results for all the cases presented previously for the RQB and SD values. Additionally, figure 34 shows the locations of the measured dof's for the TSB.

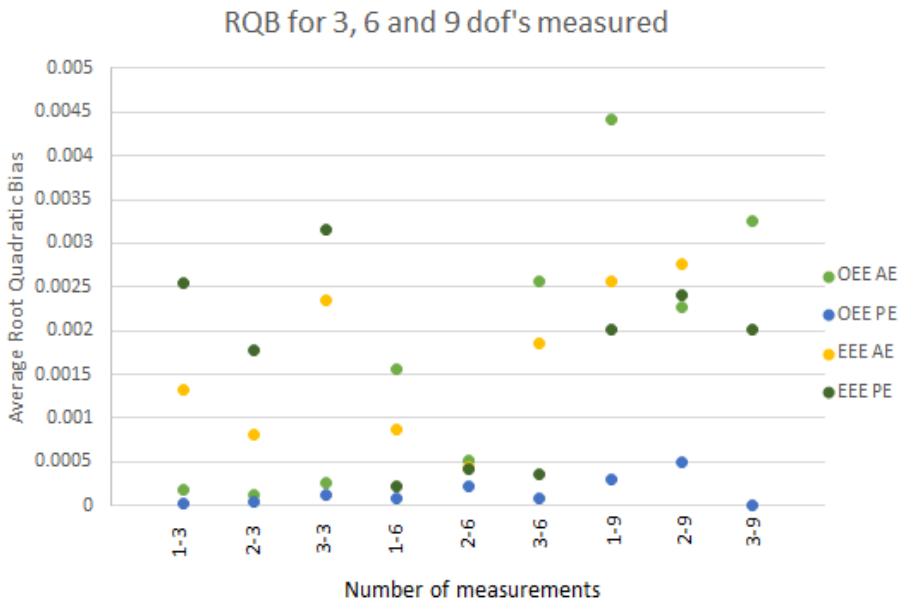

Figure 32. RQB values for TSB having 3, 6 and 9 dof's measured and 1 to 3 measurements

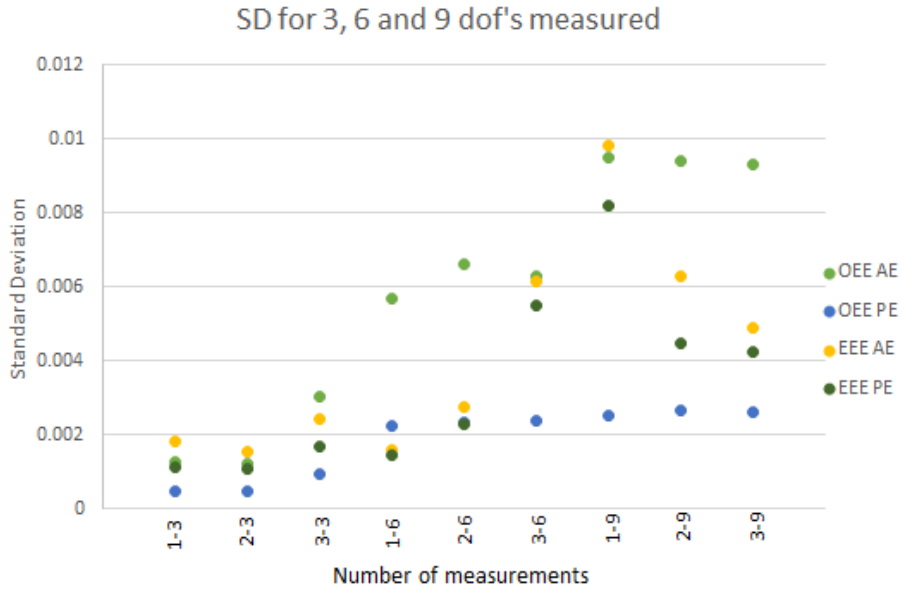

Figure 33. SD values for TSB having 3, 6 and 9 dof's measured and 1 to 3 measurements

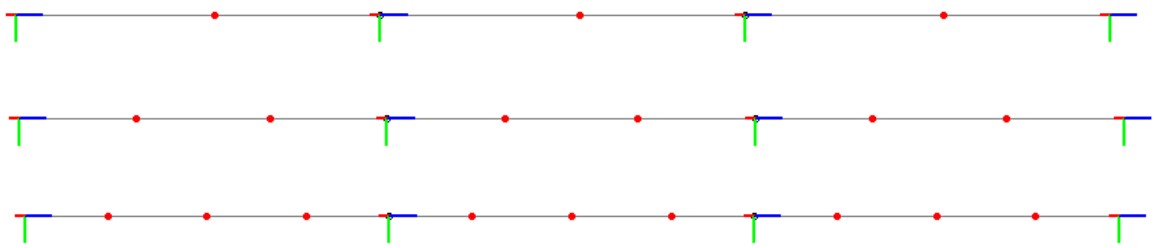

Figure 34. Location of the 3, 6 and 9 measured dof's for the TSB

Overall, RQB and SD values obtained using the OEE were lower than those obtained by the EEE for the TSB and having more data available does not necessarily mean better estimates or lower values of RQB and SD. Furthermore, it can be seen that the estimation algorithms have more sensitivity to absolute errors, due to the fact that some measurements, and especially small ones, may be controlled by a big absolute error value (λ), whereas for the proportional error, that possibility is eliminated by the use of a percent of the actual measurement as the error.

5.1.2 Estimated parameter

Table 26 presents the maximum and minimum estimated parameter (EI) of the TSB, for both the estimators and for both the error types.

Table 26. Maximum and minimum estimated parameter for the TSB

	EEE		**OEE**	
	AE	**PE**	**AE**	**PE**
Actual EI	**57,121,056,880.00 = 1.0**			
max	1.02	1.02	1.02	1.00
% Difference	1.99	1.61	1.95	0.46
min	0.99	0.99	0.99	1.00
% Difference	1.45	1.12	1.44	0.43

It can be seen from table 26 that % differences as much as 1.99 and as low as 0.43 were obtained. It is clear that the OEE gave better results than the EEE, and it did also for the case of having proportional error as opposed to having absolute error.

5.2 Parameter estimation results for the TCF Bank Stadium

Analysis of the section of the stadium was performed for different combinations of number of measurements, number of degrees of freedom (dof's) measured and different values of absolute and proportional error. The absolute error used for this analysis was from 0.01 to 0.10 and the proportional error was between 3% and 30%.

5.2.1 Statistical indices

Figures 35 and 36 show the RQB and SD values, respectively for the section of the stadium for the cases of having measured from 6 to 24 nodes (18 to 72 dof's) and having performed from 1 to 4 measurements for the EEE with absolute error. Additionally, figures 37 and 38 present the values of RQB and SD but this time with the proportional error.

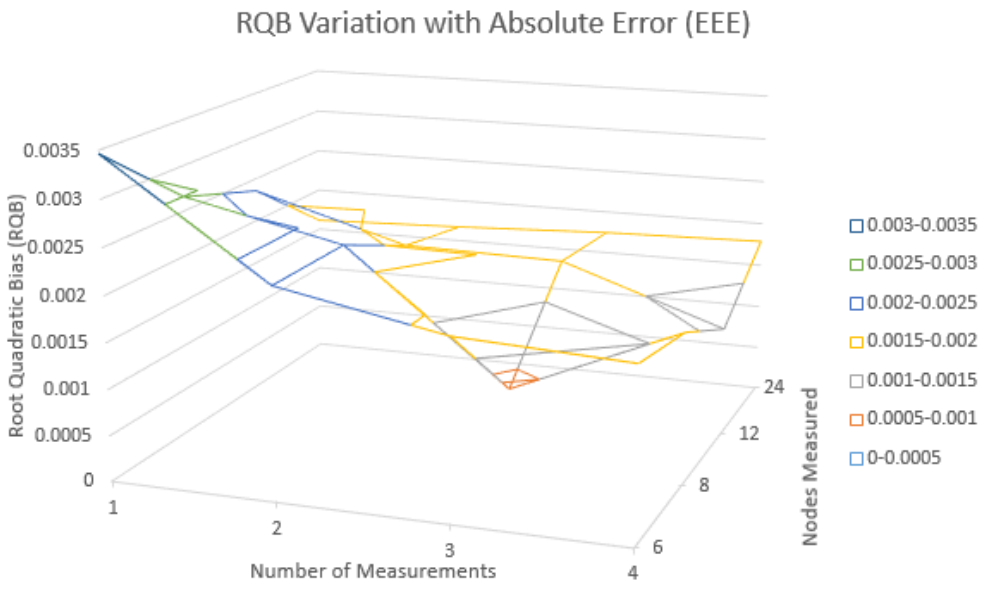

Figure 35. RQB values for the stadium having 6 to 24 nodes measured and 1 to 4 measurements with absolute error (EEE)

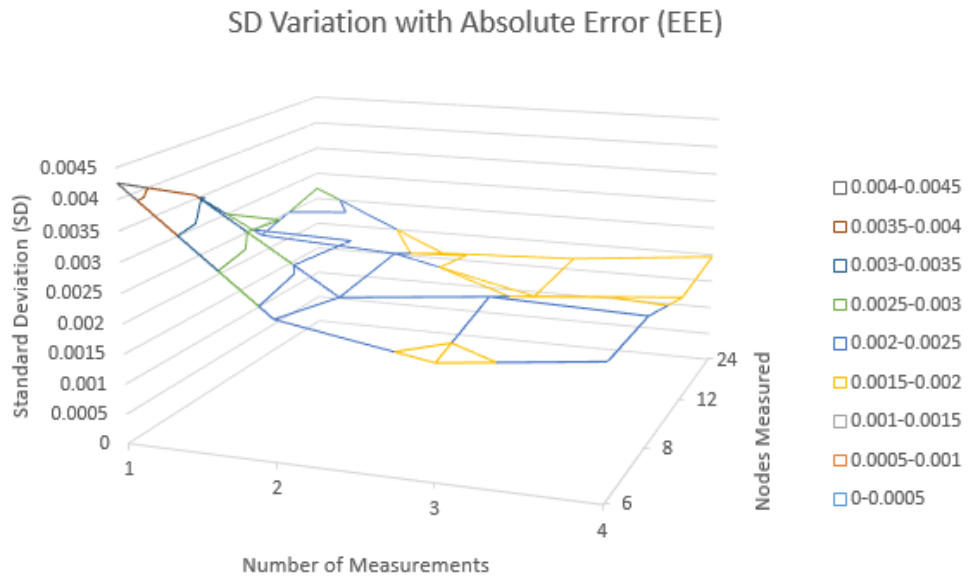

Figure 36. SD values for the stadium having 6 to 24 nodes measured and 1 to 4 measurements with absolute error (EEE)

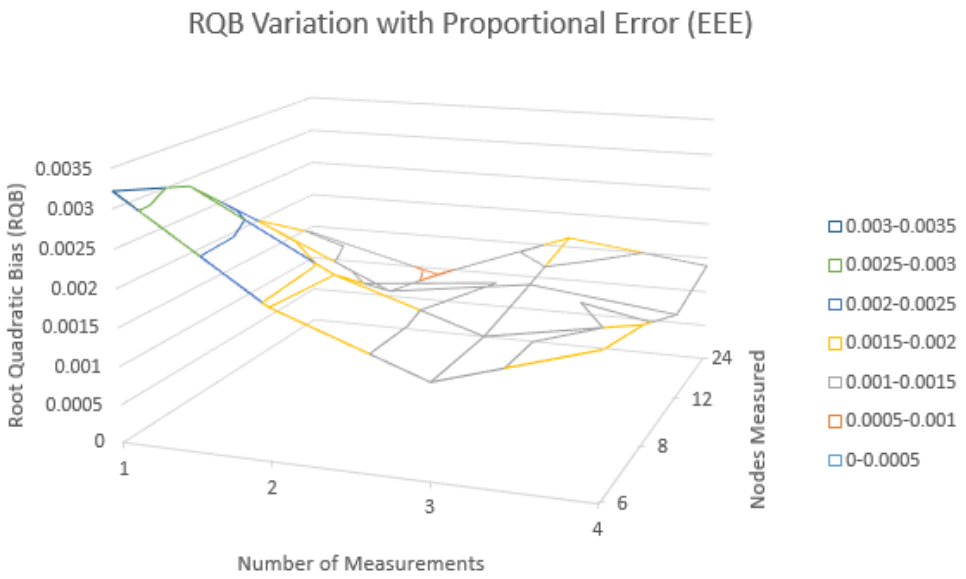

Figure 37. RQB values for the stadium having 6 to 24 nodes measured and 1 to 4 measurements with proportional error (EEE)

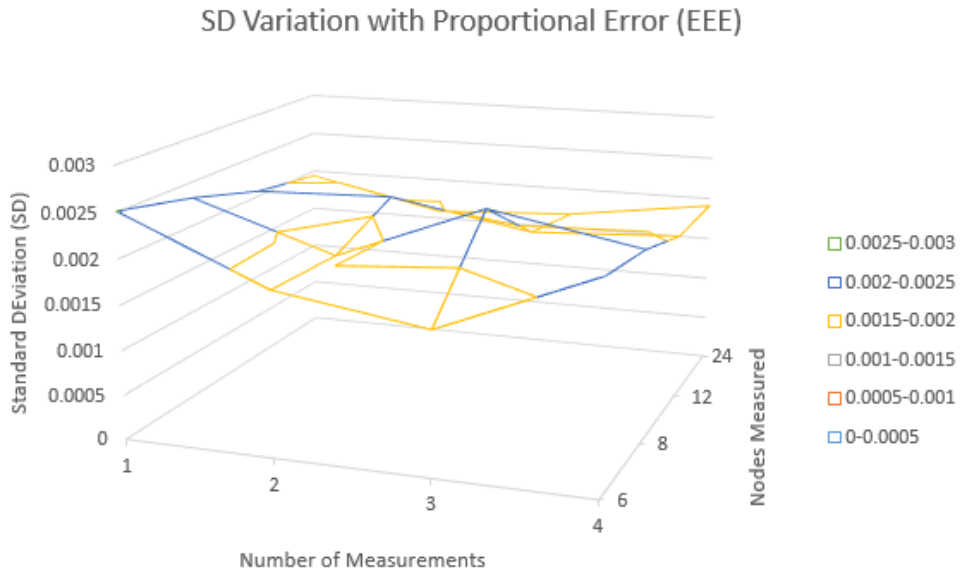

Figure 38. SD values for the stadium having 6 to 24 nodes measured and 1 to 4 measurements with proportional error (EEE)

From the previous figures it can be seen that the RQB and SD values are generally lower for the case of having introduced the proportional error. Additionally, it can be seen that the best estimates are not necessarily obtained when the full size of measurements are used (4 measurements and 24 nodes measured). For the case of having the absolute error, the best results were obtained with 3 measurements and 8 nodes measured and for the case of having proportional error, the best results were obtained with 2 measurements and 24 nodes measured.

Figures 39 and 40 show the RQB and SD values, respectively for the section of the stadium for the cases of having measured from 6 to 24 nodes and having performed from 1 to 4 measurements for the OEE with absolute error. Additionally, figures 41 and 42 present the values of RQB and SD but this time with the proportional error.

Figure 39. RQB values for the stadium having 6 to 24 nodes measured and 1 to 4 measurements with absolute error (OEE)

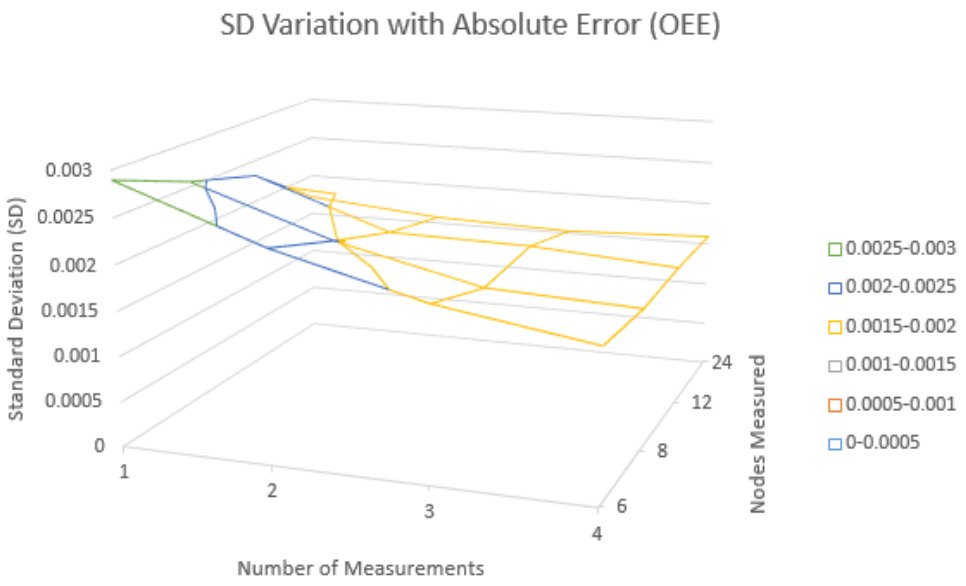

Figure 40. SD values for the stadium having 6 to 24 nodes measured and 1 to 4 measurements with absolute error (OEE)

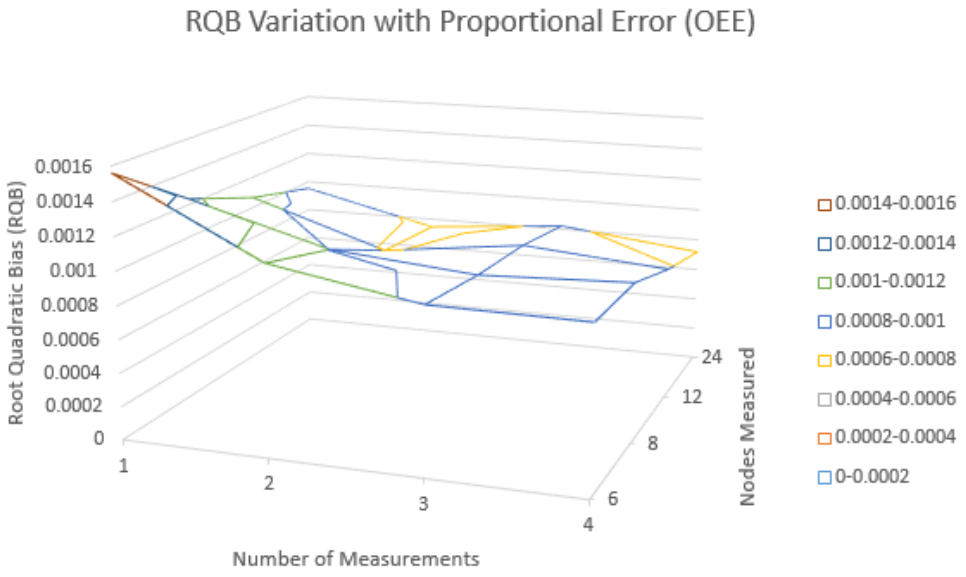

Figure 41. RQB values for the stadium having 6 to 24 nodes measured and 1 to 4 measurements with proportional error (OEE)

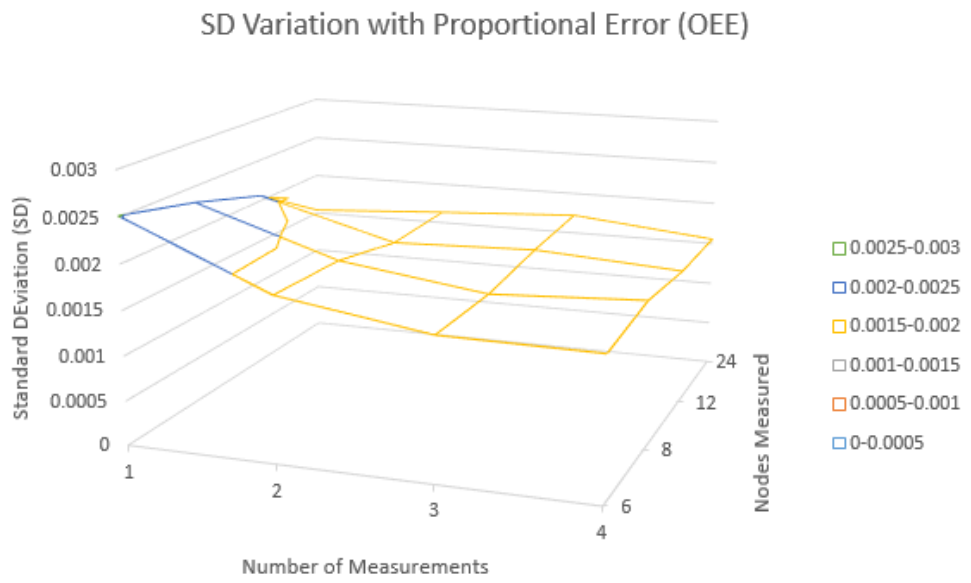

Figure 42. SD values for the stadium having 6 to 24 nodes measured and 1 to 4 measurements with proportional error (OEE)

As can be seen by the previous four figures and similar to the results from the EEE, the RQB and the SD values obtained by the OEE with proportional error are lower than those obtained with absolute error. For this estimator, it seems that having more data helps getting better and better results, except for one case where the RQB value was the least for the case of having 2 measurements and 8 nodes measured.

Comparing the results obtained from the two estimators, it can be concluded that overall the OEE gives better estimates than the EEE for the same conditions on how many measurements are done or how many nodes are measured. This could be the case because in the EEE the estimated measurements increase by a considerable amount the number of unknowns in the optimization problem.

Figures 43, 44, 45 and 46 show the location of the 6, 8, 12 and 24 measured nodes in the section of the stadium, respectively.

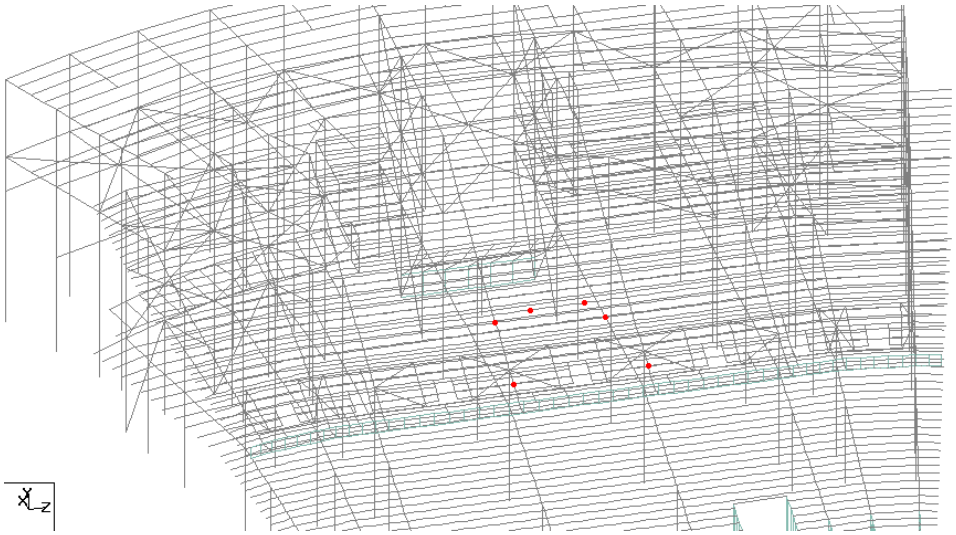

Figure 43. Location of the 6 nodes measured

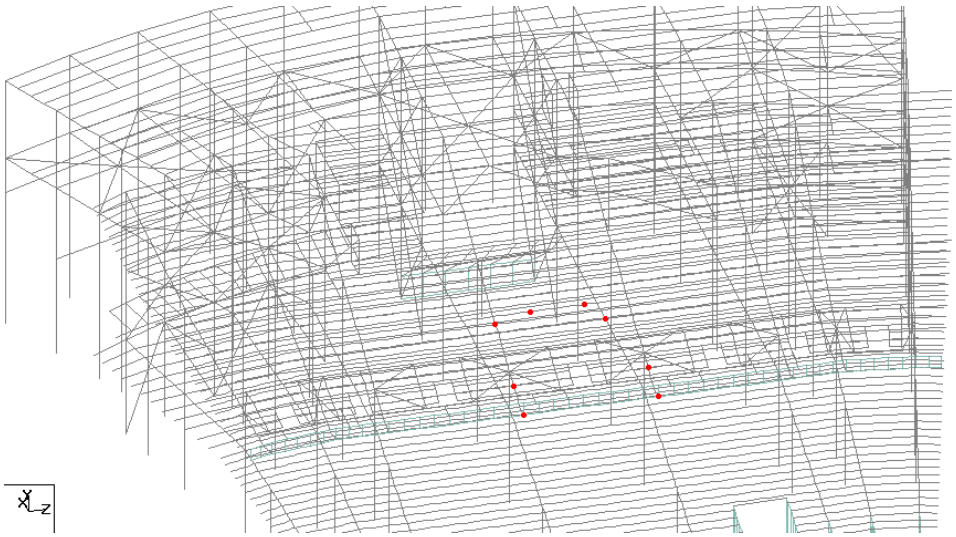

Figure 44. Location of the 8 nodes measured

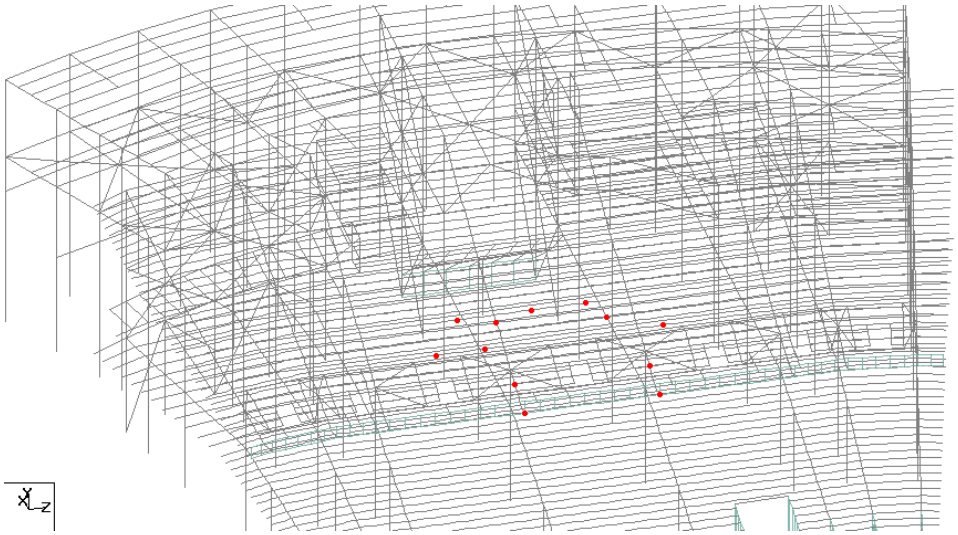

Figure 45. Location of the 12 nodes measured

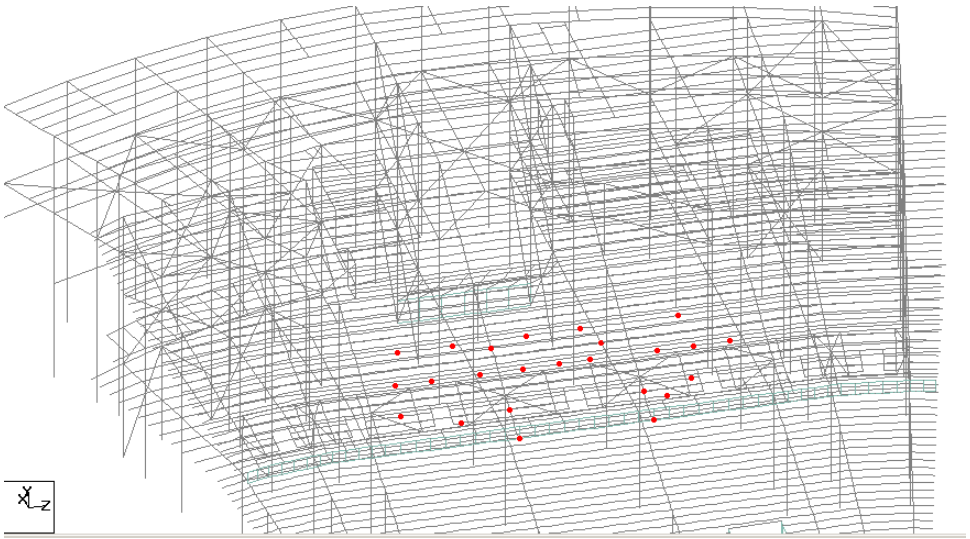

Figure 46. Location of the 24 nodes measured

5.2.2 Estimated parameters

In a similar way as was done for the TSB, the maximum and minimum estimated parameters are presented in this following section and are compared against the actual

parameters (EA, EIz, EIy), in terms of percent difference. Figure 47 shows the structural elements for which the structural parameters were estimated.

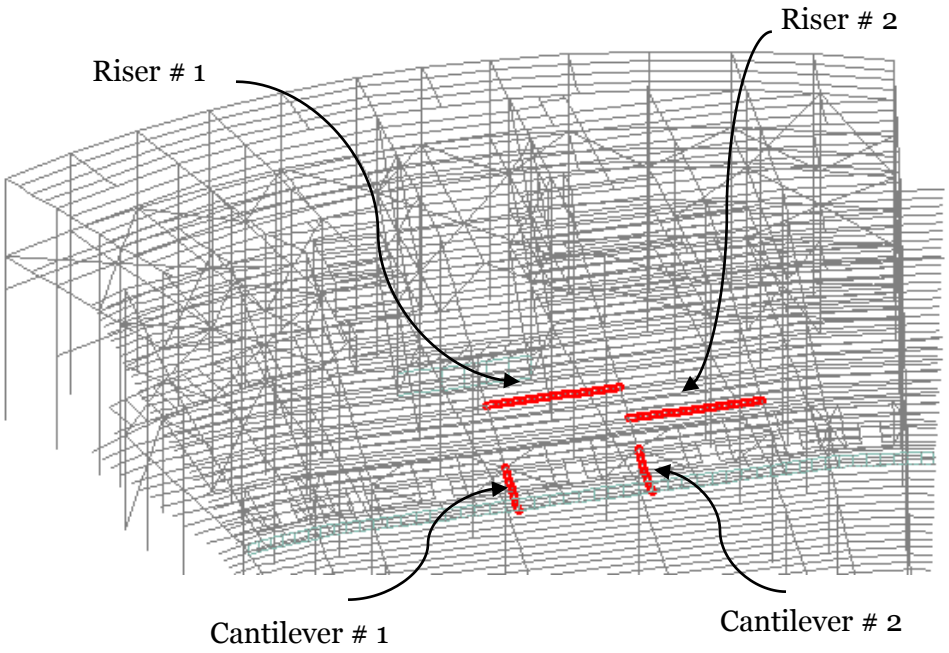

Figure 47. Structural members for which the estimated parameters are compared against the actual parameters

5.2.2.1 Estimated parameters for riser # 1

Table 27 shows the maximum and minimum estimated parameters (EA, EIz, EIy) of the section of the stadium, for both the estimators and for both the error types.

It can be seen that in general the OEE gives better results than the EEE for all of the three parameters. The maximum and minimum % difference for the EA parameter were 14.96 and 0.03, respectively. In addition, the maximum and minimum % difference for the EIz parameter were 10.68 and 6.08, respectively. Lastly, the maximum and minimum % difference for the EIy parameter were 12.55 and 2.72, respectively.

Table 27. Maximum and minimum estimated parameters of riser # 1 for the section of the stadium

	EEE		OEE	
	AE	**PE**	**AE**	**PE**
Actual EA	**1,556,639,502.06 = 1.0**			
max	1.04	1.02	1.00	1.00
% Difference	3.77	2.08	0.03	0.13
min	0.85	0.85	0.88	0.88
% Difference	14.96	14.79	12.50	12.09
Actual EIz	**57,121,056,880.00 = 1.0**			
max	1.11	1.09	1.07	1.07
% Difference	10.68	8.73	6.69	6.59
min	0.91	0.91	0.93	0.94
% Difference	9.31	8.95	6.52	6.08
Actual EIy	**198,006,270,215.00 = 1.0**			
max	1.07	1.05	1.03	1.03
% Difference	6.87	5.04	3.03	2.72
min	0.87	0.88	0.90	0.91
% Difference	12.55	12.07	9.71	9.36

5.2.2.2 Estimated parameters for riser # 2

Table 28 shows the maximum and minimum estimated parameters (EA, EIz, EIy) of the section of the stadium, for both the estimators and for both the error types.

Similar results as for riser # 1 can be seen here for riser # 2 in that the best estimates come almost always from the OEE when having a proportional error that does not change the measured dof's dramatically as the absolute error does in cases where the measured response is very small and the absolute error is comparatively larger.

The maximum and minimum % difference for the EA parameter were 15.18 and 0.15, respectively. In addition, the maximum and minimum % difference for the EIz parameter were 9.98 and 6.05, respectively. Lastly, the maximum and minimum % difference for the EIy parameter were 12.34 and 2.53, respectively.

Table 28. Maximum and minimum estimated parameters of riser # 2 for the section of the stadium

	EEE		OEE	
	AE	**PE**	**AE**	**PE**
Actual EA	**1,556,639,502.06 = 1.0**			
max	1.03	1.02	1.00	1.00
% Difference	3.11	1.92	0.28	0.15
min	0.85	0.85	0.87	0.88
% Difference	15.18	14.75	12.51	11.99
Actual EIz	**57,121,056,880.00 = 1.0**			
max	1.10	1.09	1.06	1.07
% Difference	9.98	8.67	6.17	6.52
min	0.91	0.91	0.94	0.94
% Difference	9.33	8.88	6.46	6.05
Actual EIy	**198,006,270,215.00 = 1.0**			
max	1.06	1.05	1.03	1.03
% Difference	6.28	4.96	2.53	2.75
min	0.88	0.88	0.90	0.91
% Difference	12.34	12.02	9.80	9.47

5.2.2.3 Estimated parameters for cantilever # 1

Table 29 shows the maximum and minimum estimated parameters (EA, EIz, EIy) for cantilever # 1 of the section of the stadium, for both the estimators and for both the error types.

The maximum and minimum % difference for the EA parameter were 12.01 and 5.74, respectively. In addition, the maximum and minimum % difference for the EIz parameter were 10.94 and 4.30, respectively. Lastly, the maximum and minimum % difference for the EIy parameter were 19.65 and 5.27, respectively.

The estimated parameters for cantilever # 1 were better when the OEE was used compared when the EEE was used. This behavior of the estimators is observed throughout the study, and it seems that both the estimators are more sensitive to

absolute errors. In reality, an absolute error would be present when all of the instruments deployed in the stadium have the same sensitivity and are used to measure responses of the same type and order of magnitude, but clearly one would like to have different levels of sensitivity depending on whether they are measuring vertical or horizontal displacements.

Table 29. Maximum and minimum estimated parameters of cantilever # 1 for the section of the stadium

	EEE		OEE	
	AE	**PE**	**AE**	**PE**
Actual EA	**2,297,641,800.00 = 1.0**			
max	1.10	1.09	1.06	1.08
% Difference	9.85	8.74	5.83	7.88
min	0.88	0.91	0.89	0.94
% Difference	12.01	8.53	11.45	5.74
Actual EIz	**379,158,000,000.00 = 1.0**			
max	1.11	1.08	1.06	1.04
% Difference	10.94	8.31	5.77	4.30
min	0.91	0.94	0.94	0.93
% Difference	8.82	6.21	5.84	6.72
Actual EIy	**27,571,701,600.00 = 1.0**			
max	1.10	1.08	1.06	1.05
% Difference	9.83	8.37	5.85	5.27
min	0.80	0.89	0.92	0.93
% Difference	19.65	10.78	7.81	6.61

5.2.2.4 Estimated parameters for cantilever # 2

Table 30 shows the maximum and minimum estimated parameters (EA, EIz, EIy) for cantilever # 2 of the section of the stadium, for both the estimators and for both the error types.

It can be seen that the estimated parameters for cantilever # 2 were better when the OEE with proportional error was used compared when the OEE with absolute error or when the EEE, with both types of errors, were used.

The maximum and minimum % difference for the EA parameter were 10.80 and 3.47, respectively. In addition, the maximum and minimum % difference for the EIz parameter were 12.46 and 1.31, respectively. Lastly, the maximum and minimum % difference for the EIy parameter were 13.48 and 4.62, respectively.

Table 30. Maximum and minimum estimated parameters of cantilever # 2 for the section of the stadium

	EEE		**OEE**	
	AE	**PE**	**AE**	**PE**
Actual EA	**869,145,400.00 = 1.0**			
max	1.10	1.08	1.08	1.03
% Difference	10.03	8.46	7.84	3.47
min	0.91	0.89	0.94	0.94
% Difference	8.81	10.80	6.10	5.78
Actual EIz	**20,764,830,200.00 = 1.0**			
max	1.10	1.03	1.06	1.01
% Difference	9.52	3.43	5.84	1.31
min	0.88	0.92	0.94	0.94
% Difference	12.46	8.28	5.88	5.54
Actual EIy	**10,468,469,100.00 = 1.0**			
max	1.13	1.08	1.10	1.06
% Difference	13.48	7.99	9.84	5.85
min	0.91	0.92	0.94	0.95
% Difference	8.60	8.34	5.80	4.62

5.3 Summary

Overall for the TSB, the results get better as we move from 1 measurement to two measurements, however this behavior is not observed when going from 2 to three measurements, for both the estimators. The reason for this is might be that the third

measurement does not add well enough new information for the system to obtain good values of the estimates. One thing to notice as well is that the results are better all the time proportional error is present instead of having absolute error.

Having 3 measurements and 6 dof's gives the best results in terms of the RQB values for the OEE with proportional error and the best results of SD are obtained from the EEE with proportional error with only 1 measurement.

In general, RQB and SD values obtained using the OEE were lower than those obtained by the EEE for the TSB and having more data available does not necessarily mean better estimates or lower values of RQB and SD.

Percent differences for the TSB as much as 1.99 and as low as 0.43 were obtained for the structural parameter EI. It is clear that the OEE gave better results than the EEE, and it did also for the case of having proportional error as opposed to having absolute error.

With regard to the section of the stadium, it is noted that the RQB and SD values are generally lower for the case of having introduced the proportional error. Additionally, it can be observed that the best estimates are not necessarily obtained when the full size of measurements are used. For the case of the having the absolute error, the best results were obtained with 3 measurements and 8 nodes measured and for the case of having proportional error, the best results were obtained with 2 measurements and 24 nodes measured.

Comparing the results obtained from the two estimators, it can be concluded that the OEE gives better estimates than the EEE for the same conditions on how many measurements are done or how many nodes are measured. This could be true because in

the EEE the estimated measurements increase by a considerable amount the number of unknowns in the optimization problem.

The maximum and minimum % difference for the EA parameter were 15.18 and 0.03, respectively. The maximum and minimum % difference for the EIz parameter were 10.94 and 1.31, respectively and the maximum and minimum % difference for the EIy parameter were 19.65 and 2.53, respectively, for all the four structural elements for which the comparisons were made.

For both riser # 1 and riser # 2, the best estimates come almost always from the OEE when having a proportional error that does not change the measured dof's as much as the absolute error does in cases where the measured response is very small and the absolute error is comparatively larger.

The estimated parameters for cantilever # 1 were better when the OEE was used compared when the EEE was used. It can be observed that the estimated parameters for cantilever # 2 were better when the OEE with proportional error was used compared when the OEE with absolute error or when the EEE, with both types of errors, were used.

6. CONCLUSIONS

6.1 Dynamic analysis of the TCF Bank Stadium and TSB using human-structure interaction concepts

The main conclusions that can be drawn out of the series of dynamic analyses on the TSB and the section of the stadium are as follows:

- Dynamic analysis showed that for a particular excitation frequency, the response of the TSB is greater than that produced by static analysis applying a load of 100 lb/ft^2 plus dead loads, using the load factors as per ASCE 7-10.
- The location of the passive people changes the response of the structure, either increasing or decreasing the response.
- The location of the passive people affects the response of the TSB. For the cases of 2.13 Hz and 2.30 Hz and 67% active – 33% passive produced the maximum response.
- Dynamic analysis showed that the response of some structural elements in the stadium (riser, cantilever, and girder) is sometimes greater than that obtained from static analysis.
- Reductions in the response of the stadium as much as 70% were obtained when using the different configurations (from figure 18 to figure 25) derived from the TSB, for an active/passive ratio of one.
- After applying the different configurations of active/passive people for the specific cases of having an excitation frequency of 2.13 Hz and 2.30 Hz from

figures 16 and 17 into the section of the stadium, an increase in the response, especially for the risers and girders was observed.

- Interestingly, the response in the cantilever beams of the stadium showed lower values when using the configurations from figures 16 and 17, indicating the presence of a local mode for the risers.

- Dynamic analysis using the concepts of human-structure interaction should be performed in structures that will be subjected to crowd-induced loading in order to avoid excessive deflections and vibrations that can be felt by the crowd.

6.2 Parameter estimation results

After having performed the parameter estimation study with two algorithms (EEE and OEE), the following conclusions can be made:

- RQB and SD values obtained using the OEE were lower than those obtained by the EEE for both the TSB and the stadium.

- For the TSB, having more data available does not necessarily mean better estimates or lower values of RQB and SD.

- The estimation algorithms have more sensitivity to absolute error.

- Overall, the OEE showed better results than the EEE in terms of the statistical indices and the % difference from the actual parameter values.

- For the case of the stadium and similar to the TSB case, having 4 measurements at 24 nodes does not guarantee the best estimates of the unknown parameters.

- % differences from the actual parameter values of as much as 19.65% and as low as 0.03% were obtained, meaning that the estimated parameters are in close agreement to the actual values.
- Lastly, the OEE performed better than the EEE for the great majority of the cases studied. Additionally, the presence of absolute error made the estimates less reliable due to the fact that an absolute error can overwhelm the response of dof's that have small measurements.

REFERENCES

Aktan, A.E. and Ho, I.K. (1990). “Seismic vulnerability evaluation of existing buildings”. Earthquake Spectra. 6(3). 439-472.

Bachmann, H. and Ammann, W. (1987). “Vibration in structures - induced by man and machines”. JABSE-AIPC-JVBH, Zurich.

Banan, M. R., and Hjelmstad, K. D. (1993). “Identification of structural systems from measured response.” Struct. Res. Ser. No. 579: UILU-ENG-93-2002. University of Illinois, Urbana, Ill.

Beck, J.L. (1982). “System identification applied to strong motion records from structures”. From Earthquake Ground Motion and its Effects on Structures (S.K. Dhatta, ed.) AMD Vol. 53. Proceedings of ASME Winter Annual Meeting.

Beranek, L.L. (1988). “Noise and vibration control”. Washington D.C., USA: Institute of Noise Control Engineering.

Biggs, M.C. (1972). “Constrained minimization using recursive equality quadratic programming”. Numerical Methods for Nonlinear Optimization, (Lootsma, F.A., ed.). Academic Press, London. 411-428.

Biggs, M.C. (1975). “Constrained minimization using recursive quadratic programming: some alternative subproblem formulations”. Towards Global Optimization, (Dixon, L.C.W., and Szego, G.P., eds.). North-Holland Publishing Co., Amsterdam, North-Holland.

Biggs, M.C. (1982). “Recursive quadratic programming methods for nonlinear constraints”. Nonlinear Optimization 1981, (Powell, M.J.D., ed.). Academic Press, New York. 213-221.

BRITISH STANDARDS INSTITUTION. BS 6399 Loading for Buildings. Part 1: Code of Practice for Dead and Imposed Loads. BSI, London, 1996.

Brownjohn, J.M.W. (1999). “Energy dissipation in one-way slabs with human participation”, in Proceedings of the Asia-Pacific Vibration Conference ‘99, Nanyang Technological University, Singapore, 11-13 December 1999. Vol. 1: 155-60.

Brownjohn, J.M.W. (2001). “Energy dissipation from vibrating floor slabs due to human-structure interaction”, Shock and Vibration 8(6): 315-23.

Cawley, P. (1985). “Non-destructive testing of mass produced components by natural frequency measurements”. Proc. Instn. Mech Engrs., 199(B3). 161-168.

Chen, J.C. and Garba, J.A. (1987). “On orbit damage assessment for large space structures”. Proceedings of the AIAA/ASME/ASCE/AHS 28th Structures, Structural Dynamics and Materials Conference. April. AIAA. New York, N.Y., 714-721.

Coermann, R.R. (1962). “The mechanical impedance of the human body in sitting and standing position at low frequencies”, Human factors (4): 227-53.

Coleman, T.F., and Conn, A.R. (1980). “Nonlinear programming via an exact penalty function method: asymptotic analysis”. Mathematical Programming. 24. 123-136.

Coleman, T.F., and Conn, A.R. (1980). “Nonlinear programming via an exact penalty function method: global analysis”. Mathematical Programming. 24. 137-161.

Collins, J.D., Hart, G.C., Hasselman, T.K., and Kennedy, B. (1974). “Statistical identification of structures”. AIAA J., 12(2). 185-190.

Courage, W.M.G., Schreus, P.J.G., and Janssen, J.D. (1990). “Estimation of mechanical parameter values of composites with the use of finite element and system identification techniques”. Computers & Structures. 34(2). 231-237.

DiPasquale, E. and Cakmak, A.S. (1990). “Detection of seismic structural damage using parameter-based global damaged indices”. Probabilistic Engineering Mechanics. 5(2). 60-65.

Distefano, N. and Pena-Pardo, B. (1976). “System identification of frames under seismic loads”. ASCE Journal of the Engineering Mechanics Division. 102(EM2). 313-330.

Dougill, J. W., Wright, J. R., Parkhouse, J. G. and Harrison, R.E. (2006). “Human structure interaction during rhythmic bobbing”. The Structural Engineer, pp.32-39.

Douglas, B.M. and Reid, W.H. (1982). “Dynamic tests and system identification of bridges”. ASCE Journal of Structural Division. 108(10).

Duarte, E. and Ji, T. (2009). “Action of Individual Bouncing on Structures”. Journal of Structural Engineering, ASCE, pp.818-827.

Duggan, D.M., Wallace, E.R., and Caldwell, S.R. (1980). “Measured and predicted vibrational behavior of Gulf of Mexico platform”. The 12th Annual Offshore Technology Conference. May 5-8. Houston, Texas. Paper No. OTC 3864. 91-100.

Ebrahimpour, A. and Sack, R.L. (1992) “Design live loads for coherent crowd harmonic movements”, Journal of Structural Engineering (ASCE), 118(4): 1121-36.

Ellis, B.R. and Ji, T. (1994). “Floor vibration induced by dance-type loads: theory”. The Structural Engineer Magazine 72(3): 37-44.

Ellis, B.R. and Ji, T. (1994). “Floor vibration induced by dance-type loads: verification”. The Structural Engineer Magazine 72(3): 45-50.

Ellis, B.R. and Ji, T. (1997). “Human-structure interaction in vertical vibrations”, in Proceedings of the Institution of Civil Engineers, Structures and Buildings, 122(1), pp. 1-9.

Ellis, B.R., Ji, T. and Littler, J.D. (2000). “The response of grandstands to dynamic crowd loads”. Proceedings of the Institution of Civil Engineers: Structures and Buildings, pp. 355-365.

Ellis, B.R. and Ji, T. (2004). “The response of structures to dynamic crowd loads”. Building Research Establishment Ltd. (BRE) Digest 426. 12 pages.

Ellis, J.H., Zimmerman, J.J., and Corotis, R.B. (1990). “Stochastic Programs for identifying critical structural collapse mechanisms”. Applied Mathematical Modelling.

Eykhoff, P. (1974). “System identification, parameter and state estimation”. John Wiley & Sons, Inc., New York, N.Y.

Falati, S. (1999). “The contribution of non-structural components to the overall dynamic behaviour of concrete floor slabs”. Thesis (PhD). University of Oxford, Oxford, UK.

Flannelly, W. and Berman, A. (1983). “The state of the art of system identification of aerospace structures”. AMD Vol. 59 Modal Testing and Model Refinement, (D. Chu, ed.), ASME App. Mech. Div., 121-131.

Flesch, R.G. and Kernbichler (1988). “A dynamic method for safety inspection of large prestressed bridges”. Proceeding of International Workshop on Nondestructive Evaluation for Performance of Civil Structures. University of Southern California, Los Angeles, California.

Fletcher, R. (1971). “A general quadratic programming algorithm”. Journal of Institute of Mathematics and its Applications. 7. 76-91.

Fletcher, R. (1980). “Practical methods of optimization”. Vol. 1, Unconstrained Optimization, and Vol. 2, Constrained Optimization, John Wiley and Sons.

Folz, B. and Foschi, R.O. (1991). “Coupled vibrational response of floor systems with occupants”, Journal of Engineering Mechanics (ASCE) 117(4): 872-92.

Foschi, R.O. and Gupta, A. (1987). “Reliability of floors under impact vibration”, Canadian Journal of Civil Engineering 14(5): 683-9.

Foschi, R.O., Neumann, G.A., Yao, F. and Folz, B. (1995). “Floor vibration due to occupant and reliability-based design guidelines”, Canadian Journal of Civil Engineering 22(3): 471-79.

Foster, C.D. and Mottershead, J.E. (1990). “A method for improving finite element models by using experimental data: application and implications for vibration monitoring”. Int. J. Mech. Sci., 32(3). 191-203.

Fujino, Y., Pacheo, B.M., Nakamura, S.I. and Warnitchai, P. (1993) “Synchronization of human walking observed during lateral vibration of a congested pedestrian bridge”. Earthquake Engineering and Structural Dynamics 22(9): 741-58.

Gill, P.E., Murray, W. and Wright, M.H. (1981). “Practical Optimization”, Academic Press, London.

Gill, P.E., Murray, W. and Wright, M.H. (1991). “Numerical Linear Algebra and Optimization”, Vol. 1, Addison Wesley.

Ginty, D., Derwent, J.M. and Ji, T. “The frequency range and distribution of dance type loads”. Accepted for publication in The Structural Engineer.

Goodwin, G.C. (1984). “Adaptive filtering prediction and control”. Prentice-Hall Inc., Englewood Cliffs, N.J.

Hajdasinski, A.K., Eykhoff, P. and Damen, Ad A.H. (1982). “The choice and use of different model sets for system identification”. Eindhoven: University of Technology. Internal report, Dept. EE Group ER.

Hajdasinski, A.K., Damen, Ad A.H. (1982). “Practical tests with different approximate realizations based on the singular value decomposition of the Hankel matrix”. Eindhoven: University of Technology. Internal report, Dept. EE Group ER.

Hajela, P. and Soeiro, F. (1990). “Structural damage detection based on static and modal analysis”. AIAA J., 28(6). 1110-1115.

Han, S.P. (1977). “A globally convergent method for nonlinear programming”. Journal of Optimization Theory and Applications. 22. 297-309.

Hart, G.C. and Yao, J.T.P. (1977). “System identification in structural dynamics”. ASCE Journal of the Engineering Mechanics Division. 103(EM6). 1089-1104.

Hashemi-Kia, M. (1988). “Investigation of dynamic characteristics of an elastic wings model by using corrections of mass and stiffness matrices”. Journal of Sound and Vibration. 121(1). 67-76.

Hashin, Z. (1983). “Analysis of composite materials – a survey”. Journal of Applied Mechanics. Transaction of the ASME. 50. 481-505.

Ho, I.K. and Aktan, A.E. (1989). “Linearized identification of buildings with cores for seismic vulnerability assessment”. National Center for Earthquake Engineering Research. State University of New York at Buffalo. Technical Report NCEER-89-0041.

Hollkamp, J.J. and Batill, S.M. (1991). “Automated parameter identification and order reduction for discrete time series models”. AIAA J., 29(1). 96-103.

Hothan, S. (1999). “Einfluß der Verkehrslast – Mensch – auf das Eigenschwingungsverhalten von Fußgängerbrücken und die Auslegung linearer Tilger”. Thesis (Dipl.-Ing.). Universität Hannover, Hanover, Germany.

ISO (1981). “Vibration and shock - Mechanical driving point impedance of the human body”. ISO 5982:1981. Geneva, Switzerland: International Organization for Standardization (ISO).

ISO (1987). “Mechanical vibration and shock – Mechanical transmissibility of the human body in the z direction”. ISO 7962:1987 (E). Geneva, Switzerland: ISO.

Ji, T. (1995). “A continuous model for the vertical vibration of the human body in a standing position”, in UK Informal Group Meeting on Human Response to Vibration, Silsoe, UK, 18-20 September 1995.

Ji, T. (2000). “On the combination of structural dynamics and biodynamics methods in the study of human-structure interaction”, in UK Informal Group Meeting on Human Response to Vibration, Southampton, UK, 13-15 September 2000. 183-94.

Ji, T. and Ellis, B.R. (1993). “Evaluation of dynamic crowd effects for dance type loads”. Colloquium on Structural Serviceability of Buildings, Goteborg, pp. 165-172.

Jiang, J.S., Gu, S.N., Wang, Y.J., and Yao, Q.H. (1990). “A modal parameter identification technique and its application to large complex structures with multiple steady sinusoidal excitation”. Journal of Sound and Vibration. 138(2). 221-231.

Kammer, D., Jensen, B., and Mason, D. (1988). “Test-analysis correlation of the space shuttle solid rocket motor center segment”. Proceedings of the AIAA/ASME/ASCE/AHS 29th Structures, Structural Dynamics and Materials Conference, Part 3. AIAA. April 18-20. 1474-1486.

Kasperski, M. and Niemann, H.J. (1993). “Man induced vibrations of a stand structure”, in Moan, T., et al. (eds) EURODYN’93, Trondheim, Norway. Rotterdam, The Netherlands: A.A. Balkema Publishers. 977-983.

Kasperski, M. (1996). Actual problems with stand structures due to spectator induced vibrations. EURODYN’96, Florence, 455-461.

Kenley, R.M. and Dodds, C.J. (1980). “West sole we platform: detection of damage by structural response measurements”. The 12th Annual Offshore Technology Conference. May 5-8. Houston, Texas. Paper No. OTC 3866. 111-118.

Lenzing, H. (1988). “Durch Menschen induzierte Schwingungen”. Thesis (Dipl.-Ing.). Universität Hannover, Hanover, Germany.

Littler, J. D. (2000). “Retractable Grandstands: Dynamic Response”. Building Research Establishment, Watford, 2000, BRE IP 4/00.

Ljung, L. and Glover, K. (1981). “Frequency domain versus time domain methods in system identification”. Automatica, 17(1), 71-90.

Luenberger, D.G. (1989). “Linear and Nonlinear Programming”. Addison-Wesley Publishing Co.

Matko, D. and Schumann, R. (1982). “Comparative stochastic convergence analysis of seven recursive parameter estimation methods”. Proceedings of the sixth IFAC Symposium. June. Washington, D.C.

Mottershead, J.E. (1990). “Theory for the estimation of structural vibration parameters from incomplete data”. AIAA J., 28(3). 559-561.

Murray, W. (1969). “An algorithm for constrained minimization”. Optimization, (Fletcher, R., ed.). Academic Press, London. 247-258.

Murray, W., and Wright, M.H. (1978). “Projected Lagrangian methods based on the trajectories of penalty barrier functions”. Report SOL 78-23, Department of Operations Research, Stanford University. Stanford, California.

Murray, W., and Wright, M. H. (1982). “Computation of the search direction in constrained optimization algorithm”. Mathematical Programming Study. 16. 62-83.

Natke, H.G. (1989). “Identification approaches in damage detection and diagnosis”. Diagnostics. Politechnika Poznanska, Rydzyna.

Niederlinski, A., Hajdasinski, A. K. (1979). “Multivariable system identification: a survey”. 5th IFAC Symposium on identification and system parameter estimation.

Nigam, S.P. and Malik, M (1987). “A study on a vibratory model of a human body”, Journal of Biomechanical Engineering 109(2): 148-53.

Ortiz, A., Gomez, D. and Thomson, P. (2009). “Caracterización del efecto de la interacción Humano-Estructura en el Estadio Olímpico en Cali, Colombia” (Characterising the human structure interaction effect of the Olympic Stadium in Cali, Colombia). Engineering and Research Magazine 29(1): 13-23.

Parkhouse, J. G. and Ewins, D. J. (2006). “Crowd induced rhythmic loading”. Proceedings of the Institution of Civil Engineers: Structures and Buildings. SB5, pp.247-259.

Powell, M.J.D. (1978). “A fast algorithm for nonlinearly constrained optimization calculation”. Numerical Analysis, Dundee, 1977, (Watson, G.A., ed.). Springer-Verlag, Berlin. 144-157.

Powell, M.J.D. (1983). “Variable Metric Methods for Constrained Optimization”, Mathematical Programming: The State of the Art, (A. Bachem, M. Grotschel and B.Korte, eds.) Springer Verlag, pp. 288-311.

Raghavendrachar, M. Shelley, S.J., and Aktan, A.E. (1991). “Modal test by impact for bridge diagnosis”. Unpublished.

Randall, J.M. and Peng, C. (1995). “Vibrating beam method for measuring animal natural frequencies”, Journal of Low Frequency Noise and Vibration 14(3): 119-33.

Reynolds, P., Pavic, A. and Ibrahim, Z. (2004). “The effects of crowd occupation on the dynamic performance of a grandstand”. Proceedings of the International Conference on Noise and Vibration Engineering, pp. 797-810.

Sachse, R. (2002). “The influence of human occupants on the dynamic properties of slender structure”, Ph.D. Thesis, The University of Sheffield, UK, April 2002, ISBN: 3-936231-71-0.

Sachse, R., Pavic, A. and Reynolds, P. (2002). “The influence of a group of humans on the properties of a structure”, in H. Grundmann and G.I. Schuëller, Editors, Proceedings of the 5th European Conference on Structural Dynamics (Eurodyn 2002), Munich, Germany, 2002 September 2 5, A. A. Balkema (2002), pp. 1241-1246.

Sachse, R., Pavic, A. and Reynolds, P. (2003). “Human-Structure Dynamic Interaction in Civil Engineering Dynamics: A Literature Review”. Engineering and Physical Sciences Research Council (EPSRC).

Schittowski, K. (1985). “NLQPL: A FORTRAN-Subroutine Solving Constrained Nonlinear Programming Problems”, Annals of Operations Research, Vol. 5, pp. 485-500.

Schneider, M. (1991). “Ein Beitrag zu fußgängerinduzierten Brückenschwingungen”. Thesis (PhD). Technische Universität München, Munich, Germany. (Contribution to pedestrian induced vibrations of bridges).

Sheena, Z., Unger, A., and Zalmanovich, A. (1982). “Theoretical stiffness matrix correction by using static test results”. Israel Journal of Technology. 20. 245-253.

Sim, J.H.H. (2006). “Human-Structure Interaction in Cantilever Grandstands”. A thesis submitted for the degree of Doctor of Philosophy at the University of Oxford.

Soeiro, F.J. and Hajela, P. (1990). “Damage detection in composite materials using identification techniques”. AIAA Paper No. 90-0917-CP. 950-960.

Struck, W. and Limberger, E. (1981) “Die stoßartige Beanspruchung horizontaler Bauteile durch einen mit den Füßen aufprallenden Menschen”, Die Bautechnik 58(10): 347-51.

Stubbs, N., Broome, T.H., and Osegueda, R. (1989). “Nondestructive construction error detection in large space structures”. AIAA J., 28(1). 146-152.

Suggs, C.W., Abrams, C.F. and Stikeleather, L.F. (1969). “Equipment note: Application of a damped spring-mass human vibration simulator in vibration testing of vehicle seats”, Ergonomics 12(1): 79-90.

Supplement to the National Building Code of Canada: No. 1, “Commentary A: serviceability criteria for deflections and vibrations”, Ottawa, National Research Council of Canada, 1985.

Thoren, A.R. (1972). “Derivation of mass and stiffness from dynamic test data”. AIAA/ASME/SAE 13th Structures, Structural Dynamics and Materials Conference. April 10-12. San Antonio, Texas. AIAA Paper No. 72-346.

Torkamani, M.A.M. and Ahmadi, M.K. (1988). “Stiffness identification of two and three dimensional frames”. Earthquake Engineering and Structural Dynamics. 16(8). 1157-1176.

Torkamani, M.A.M. and Ahmadi, M.K. (1988). “Stiffness identification of a tall building during construction period using ambient tests”. Earthquake Engineering and Structural Dynamics. 16. 1177-1188.

Torkamani, M.A.M. and Ahmadi, M.K. (1988). “Stiffness identification of framed using simulated ground excitation”. ASCE Journal of Engineering Mechanics. 114(5). 753-776.

Tuan, C. Y. and Saul, W. E. (1985). “Loads due to spectator movements”. Journal of Structural Engineering, ASCE, 111(2), pp. 418-434.

Tustin, W. and Mercado, R. (1985). “Machinery health monitoring - an application of spectrum analysis”. Journal of Society of Environmental Engineers. 17-22.

van Staalduinen, P. and Courage, W. (1994) “Dynamic loading of Feyenoord stadium during pop concerts”, in Symposium: Places of Assembly and Long-Span Building Structures, Birmingham, UK, 7-9 September, 1994. Zürich, Switzerland: IABSE. Report 71: 283-8.

Vandiver, J.K. (1975). “Detection of structural failure on fixed platforms by measurement of dynamic response”. The 7th Annual Offshore Technology Conference. May 5-8. Houston, Texas. OTC 2267. 243-252.

Wei, L. and Griffin, M.J. (1998). “Mathematical models for the apparent mass of the seated human body exposed to vertical vibration”, Journal of Sound and Vibration 212(5): 855-74.

Werner, S.D., Douglas, B.M., and Course, C.B. (1989). “System identification of Meloland road overcrossing”. Seismic Engineering: Research and Practice, Proceeding of Sessions Related to Seismic Engineering at Structures Congress. San Francisco, California.

Williams, C., Rafiq, M.Y. and Carter, A. (1999). “Human structure interaction: The development of an analytical model of the human body”, in Vibration, Noise and Structural Dynamics. Venice, Italy, 28-30 April 1999. Staffordshire, UK: Staffordshire University Press. 32-9.

Yang, Y. (2010). “Comparison of Bouncing Loads Provided by Three Different Human Structure Interaction Models”. 978-1-4244-7739-5, IEEE.

Zadeh, L. A. (1962). “From circuit theory to system theory”. Proc. IRE. 50. 856-865.

Zhang, W.C. and Evans, K.E. (1988). “Numerical prediction of the mechanical properties of anisotropic composite materials”. Computers & Structures. 29. 413-422.

Zheng, X. and Brownjohn, J.M.W. (2001). “Modeling and simulation of human-floor system under vertical vibration”, in Davis, L.P. (ed) Smart Structures and Material 2001: Smart Structures and Integrated Systems. Proceedings of SPIE, Vol. 4327: 513-20.

Zienkiewicz, O.C. (1977). “A new look at the Newmark, Houbolt, and other time stepping formulas. A weighted residual approach”. Earthquake Engineering and Structural Dynamics. 5. 413-418.

Zimoch, Z. (1987). “Sensitivity analysis of vibrating systems”. Journal of Sound and Vibration. 115(3). 447-458.

APPENDIX A

CONSTRAINED OPTIMIZATION PROBLEM

SQP methods represent state-of-the-art in nonlinear programming methods. Schittowski (1985), for example, has implemented and tested a version that out performs every other tested method in terms of efficiency, accuracy, and percentage of successful solutions, over a large number of test problems.

Based on the work of Biggs (1975), Han (1977), and Powell (1978), the method allows anyone to closely mimic Newton's method for constrained optimization just as is done for unconstrained optimization. At each major iteration an approximation is made of the Hessian of the Lagrangian function using a quasi-Newton updating method. This is then used to generate a QP sub-problem whose solution is used to form a search direction for a line search procedure. An overview of SQP is found in Fletcher (1980), Gill et al. (1981), Powell (1983). The general method, however, is stated here. Given the problem description in Eqn. A.1 the principal idea is the formulation of a QP sub-problem based on a quadratic approximation of the Lagrangian function.

$$\begin{aligned} &\min_{x\in\Re^n} imize && f(x) \\ &\text{Subject to:} && G_i x = 0 && i = 1,\ldots,m_e \\ &&& G_i(x) \le 0 && i = m_e+1,\ldots,m \\ &&& x_l \le x \le x_u \end{aligned} \tag{A.1}$$

Where x is the vector of design parameters, f(x) is the objective function that returns a scalar value, and the vector function G(x) returns the values of the equality and inequality constraints evaluated at $x\left(G(x):\Re^n \to \Re^m\right)$.

$$L(x,\lambda) = f(x) + \sum_{i=1}^{m} \lambda_i \cdot g_i(x) \tag{A.2}$$

Here Eqn. A.1 is simplified by assuming that bound constraints have been expressed as inequality constraints. The QP sub-problem is obtained by linearizing the nonlinear constraints.

QP Subproblem

$$\min_{d \in \Re^n} imize \qquad \frac{1}{2} d^T H_k d + \nabla f(x_k)^T d$$

$$\nabla g_i(x_k)^T d + g_i(x_k) = 0 \qquad i = 1,..m_e \tag{A.3}$$

$$\nabla g_i(x_k)^T d + g_i(x_k) \le 0 \qquad i = m_e + 1,..m$$

This sub-problem can be solved using any QP algorithm. The solution is used to form a new iterate $x_{k+1} = x_k + \alpha_k d_k$

The step length parameter α_k is determined by an appropriate line search procedure so that a sufficient decrease in a merit function is obtained. The matrix H_k is a positive definite approximation of the Hessian matrix of the Lagrangian function (Eqn. A.2). H_k can be updated by any of the quasi-Newton methods, although the BFGS method appears to be the most popular.

A nonlinearly constrained problem can often be solved in fewer iterations than an unconstrained problem using SQP. One of the reasons for this is that, because of limits on the feasible area, the optimizer can make well-informed decisions regarding directions of search and step length.

SQP Implementation

The MATLAB SQP implementation consists of three main stages, which are discussed briefly in the following sub-sections:

- Updating of the Hessian matrix of the Lagrangian function

- Quadratic programming solution
- Line search and merit function calculation

Updating the Hessian Matrix

At each major iteration a positive definite quasi-Newton approximation of the Hessian of the Lagrangian function, *H*, is calculated using the BFGS method where *i* (*i* = 1,...,*m*) is an estimate of the Lagrange multipliers.

Hessian Update (BFGS)

$$H_{k+1} = H_k + \frac{q_k q_k^T}{q_k^T s_k} - \frac{H_k^T H_k}{s_k^T H_k s_k}$$

$$s_k = x_{k+1} - x_k \tag{A.4}$$

$$q_k = \nabla f(x_{k+1}) + \sum_{i=1}^{n} \lambda_i \cdot \nabla g_i(x_{k+1}) - \left(\nabla f(x_k) + \sum_{i=1}^{n} \lambda_i \cdot \nabla g_i(x_k) \right)$$

Powell (1978) recommends keeping the Hessian positive definite even though it may be positive indefinite at the solution point. A positive definite Hessian is maintained providing $q_k^T s_k$ is positive at each update and that *H* is initialized with a positive definite matrix. When $q_k^T s_k$ is not positive, q_k is modified on an element by element basis so that $q_k^T s_k > 0$. The general aim of this modification is to distort the elements of q_k , which contribute to a positive definite update, as little as possible. Therefore, in the initial phase of the modification, the most negative element of $q_k * s_k$ is repeatedly halved. This procedure is continued until $q_k^T s_k$ is greater than or equal to 1*e*-5. If after this procedure, $q_k^T s_k$ is still not positive, q_k is modified by adding a vector *v* multiplied by a constant scalar *w*, that is,

$$q_k = q_k + wv \tag{A.5}$$

$$v_i = \nabla g_i(x_{k+1}) \cdot g_i(x_{k+1}) - \nabla g_i(x_k) \cdot g_i(x_k),$$

Where $v_i = 0$ if $(q_k)_i \cdot w < 0$ and $(q_k)_i \cdot (s_k)_i < 0$ otherwise $(i = 1,..m)$

And w is systematically increased until $q_k^T s_k$ becomes positive.

Quadratic Programming Solution

At each major iteration of the SQP method a QP problem is solved of the form where A_i refers to the ith row of the m-by-n matrix A.

$$\min_{d \in \Re^n} imize \qquad q(d) = \frac{1}{2} d^T H d + c^T d$$

$$A_i d = b_i \qquad i = 1,..m_e \tag{A.6}$$

$$A_i d \le b_i \qquad i = m_e + 1,..m$$

The method used in the Optimization Toolbox is an active set strategy (also known as a projection method) similar to that of Gill et al. (1991). It has been modified for both LP and QP problems.

The solution procedure involves two phases: the first phase involves the calculation of a feasible point (if one exists), the second phase involves the generation of an iterative sequence of feasible points that converge to the solution. In this method an active set is maintained, A_k, which is an estimate of the active constraints (i.e., which are on the constraint boundaries) at the solution point. Virtually all QP algorithms are active set methods. This point is emphasized because there exist many different methods that are very similar in structure but that are described in widely different terms.

A_k is updated at each iteration, *k*, and this is used to form a basis for a search direction $\hat{d}_k$. Equality constraints always remain in the active set, A_k. The notation for the variable, $\hat{d}_k$,is used here to distinguish it from d_k in the major iterations of the SQP method. The search direction, $\hat{d}_k$, is calculated and minimizes the objective function while remaining on any active constraint boundaries. The feasible subspace for $\hat{d}_k$ is formed from a basis, Z_k whose columns are orthogonal to the estimate of the active set A_k. Thus a search direction, which is formed from a linear summation of any combination of the columns of Z_k, is guaranteed to remain on the boundaries of the active constraints.

The matrix Z_k is formed from the last m-l columns of the QR decomposition of the matrix A_k, where l is the number of active constraints and l < m. That is, Z_k is given by

$$Z_k = Q[:, l+1:m] \qquad \text{Where } Q^T A_k^T = \begin{bmatrix} R \\ 0 \end{bmatrix} \tag{A.7}$$

Having found Z_k, a new search direction $\hat{d}_k$ is sought that minimizes q(d) where $\hat{d}_k$ is the null space of the active constraints, that is, $\hat{d}_k$ is a linear combination of the columns of Z_k: $\hat{d}_k = Z_k p$ for some vector p. Then if we view our quadratic as a function of p, by substituting for $\hat{d}_k$, we have

$$q(p) = \frac{1}{2} p^T Z_k^T H Z_k p + c^T Z_k p \tag{A.8}$$

Differentiating this with respect to p yields

$$\nabla q(p) = Z_k^T H Z_k p + Z_k c \tag{A.9}$$

$\nabla q(p)$ is referred to as the projected gradient of the quadratic function because it is the gradient projected in the subspace defined by Z_k. The term $Z_k^T H Z_k$ is called the projected Hessian. Assuming the Hessian matrix H is positive definite, then the minimum of the function q(p) in the subspace defined by Z_k occurs when $\nabla q(p) = 0$, which is the solution of the system of linear equations

$$Z_k^T H Z_k p = -Z_k^T c \tag{A.10}$$

A step is then taken of the form

$$x_{k+1} = x_k + \alpha \hat{d}_k \qquad \text{where} \quad \hat{d}_k = Z_k^T p \tag{A.11}$$

At each iteration, because of the quadratic nature of the objective function, there are only two choices of step length α. A step of unity along $\hat{d}_k$ is the exact step to the minimum of the function restricted to the null space of A_k. If such a step can be taken, without violation of the constraints, then this is the solution to QP (Eqn. A.7). Otherwise, the step along $\hat{d}_k$ to the nearest constraint is less than unity and a new constraint is included in the active set at the next iterate. The distance to the constraint boundaries in any direction $\hat{d}_k$ is given by

$$\alpha = \min_i \left\{ \frac{-(A_i x_k - b_i)}{A_i \hat{d}_k} \right\} \qquad (i = 1,\ldots,m) \tag{A.12}$$

Which is defined for constraints not in the active set, and where the direction $\hat{d}_k$ is towards the constraint boundary. When n independent constraints are included in the active set, without location of the minimum, Lagrange multipliers, λ_k are calculated that satisfy the nonsingular set of linear equations

$$A_k^T \lambda_k = c \tag{A.13}$$

If all elements of λ_k are positive, x_k is the optimal solution of QP (Eqn. A.7). However, if any component of λ_k is negative, and it does not correspond to an equality constraint, then the corresponding element is deleted from the active set and a new iterate is sought.

Initialization

The algorithm requires a feasible point to start. If the current point from the SQP method is not feasible, then a point can be found by solving the linear programming problem

$$\begin{aligned} \underset{\gamma\in\Re, x\in\Re^n}{\min imize} \quad & \gamma \\ A_i x = b_i \quad & i = 1,\ldots,m_e \\ A_i x - \gamma \le b_i \quad & i = m_e+1,\ldots,m \end{aligned} \tag{A.14}$$

The notation A_i indicates the ith row of the matrix A. A feasible point (if one exists) to Eqn. A.14 can be found by setting x to a value that satisfies the equality constraints. This can be achieved by solving an under- or over-determined set of linear equations formed from the set of equality constraints. If there is a solution to this problem, then the slack variable γ is set to the maximum inequality constraint at this point.

The above QP algorithm is modified for LP problems by setting the search direction to the steepest descent direction at each iteration where g_k is the gradient of the objective function (equal to the coefficients of the linear objective function)

$$\hat{d}_k = -Z_k Z_k^T g_k \tag{A.15}$$

If a feasible point is found using the above LP method, the main QP phase is entered. The search direction $\hat{d}_k$ is initialized with a search direction $\hat{d}_1$ found from solving the set of linear equations

$$H\hat{d}_1 = -g_k \tag{A.16}$$

Where g_k is the gradient of the objective function at the current iterate x_k. If a feasible solution is not found for the QP problem, the direction of search for the main SQP routine $\hat{d}_k$ is taken as one that minimizes γ.

Line Search and Merit Function

The solution to the QP sub-problem produces a vector d_k, which is used to form a new iterate

$$x_{k+1} = x_k + \alpha d_k \tag{A.17}$$

The step length parameter α_k is determined in order to produce a sufficient decrease in a merit function. The following merit function has been used in this implementation

Merit function

$$\Psi(x) = f(x) + \sum_{i=1}^{m_0} r_i \cdot g_i(x) + \sum_{i=m_0+1}^{m} r_i \cdot \max\{0, g_i(x)\} \tag{A.18}$$

Powell recommends setting the penalty parameter

$$r_i = (r_{k+1})_i = \max_i \left\{ \lambda_i, \frac{1}{2}\left((r_k)_i + \lambda_i\right) \right\} \qquad i = 1,\ldots,m \tag{A.19}$$

This allows positive contribution from constraints that are inactive in the QP solution but were recently active. In this implementation, initially the penalty parameter r_i is set to

$$r_i = \frac{\|\nabla f(x)\|}{\|\nabla g_i(x)\|} \tag{A.20}$$

Where $\| \ \|$ represents the Euclidean norm.

This ensures larger contributions to the penalty parameter from constraints with smaller gradients, which would be the case for active constraints at the solution point.